Reservoir-assisted quantum battery charging at finite temperatures

Y. Yao¹ and X. Q. Shao^{2,3,*}

¹School of Science, Shenyang Ligong University, Shenyang 110159, China
²Center for Quantum Sciences and School of Physics, Northeast Normal University, Changchun 130024, China
³Center for Advanced Optoelectronic Functional Materials Research,
and Key Laboratory for UV Light-Emitting Materials and Technology of Ministry of Education,
Northeast Normal University, Changchun 130024, China

Quantum batteries, as highly efficient energy storage devices, have garnered significant research interest. A key challenge in their development is to maximize the extractable energy (ergotropy) when operating within a finite-temperature reservoir. To address this, we applied quantum feedback control to the charger and investigated the effects of fermionic and bosonic thermal reservoirs on the performance of quantum batteries, including stored energy, ergotropy, and charging efficiency, in an open environment. Our findings reveal that, regardless of the type of thermal reservoir, the system exhibits optimal charging parameters. In particular, in a fermionic thermal reservoir, increasing the environmental temperature enhances battery performance, enabling stable and efficient charging. In contrast, within a bosonic thermal reservoir, higher temperatures hinder energy storage and extraction, significantly reducing charging efficiency. Additionally, we explored the impact of battery size and found that, under a fermionic reservoir, increasing the battery size appropriately can further improve performance.

I. INTRODUCTION

The growing demand for energy resources and the increasing environmental challenges have sparked a growing interest in the investigation of revolutionary energy storage and supply devices. The researchers anticipate that by integrating experimental techniques for precise detection and manipulation at the qubit level, they can realize a new principle of the energy storage and supply device —quantum battery [1]. Unlike traditional batteries, which convert chemical energy or other forms of energy storage into electricity, quantum batteries store energy based on the principles of quantum mechanics, typically in the form of excited states of quantum systems. At present, quantum batteries have been explored in a variety of physical systems, including atoms and molecules [2–6], spin [7–17], transmon [18–20], and micromaser [21–23], etc. They are expected to be smaller, possess a higher charging power [24–38], higher charging capacity [39–48], and offer a greater amount of extractable work [49–57] compared to traditional batteries.

Open quantum batteries, which are closer to practical application scenarios, have greater research value than ideal closed quantum batteries, but they face several challenges. For example, environmental-induced decoherence causes the stored energy in quantum batteries to spontaneously dissipate, leading to battery aging and reduced charging efficiency [58]. Additionally, a finite-temperature environment will cause the battery to tend toward a passive state, thereby hindering the extraction of energy from the quantum battery [59–61]. In short, as a cutting-edge technology, the quantum battery has made progress in theory and experiment [62–70], but to realize its commercialization and large-scale application, many technical challenges remain to be overcome, including environmental decoherence and energy extraction efficiency.

Considering the potential impact of environmental factors on the charging performance of the battery, researchers have designed a variety of charging schemes. These include using adiabatic [65, 71–74], measurement [75–79], and control technique [80–84] to develop the corresponding strategies that ensure open quantum batteries can be charged stably and efficiently. Several schemes utilizing Floquet engineering [85] and environment engineering [86–96] aim to beat the decoherence effects. In addition, some researchers have also paid attention to the influence of temperature on the performance of quantum batteries. For example, Song et al. [97] studied the extractable work and conversion efficiency of a quantum battery in the presence of a bosonic or fermionic thermal reservoir using the entropy uncertainty relation. Under the positive temperature mechanism, the temperature reduces the energy extraction and conversion efficiency of the battery. A feature of the aforementioned studies is that they treat the battery as an ideal non-dissipative model, whereas the dissipation of the battery itself should be accounted for in practical scenarios. Kamin et al. [98] studied the steady-state charging process of a single-cell quantum battery embedded in the center of a star comprising N qubits, under two different equilibrium and non-equilibrium scenarios. The results indicate that high-temperature has a detrimental effect across all parameter ranges, inhibiting the battery's energy extraction. Quach et al. [99] used dark states to design quantum batteries with both superextensive capacity and power density. However, an increase in temperature is detrimental to energy storage in the quantum battery and reduces the upper limit of the battery's energy extraction. Cruz et al. [100] put forward a feasible realization of a quantum battery based on carboxylate metal complexes. The scheme demonstrates that temperature hinders battery energy extraction, with the extracted energy being 75% of its corresponding maximum at room temperature. Therefore, improving the maximum extractable energy and charging efficiency of the battery in finite-temperature reservoirs remains a challenge to address.

In this work, our objective was to design an open quan-

^{*} shaoxq644@nenu.edu.cn

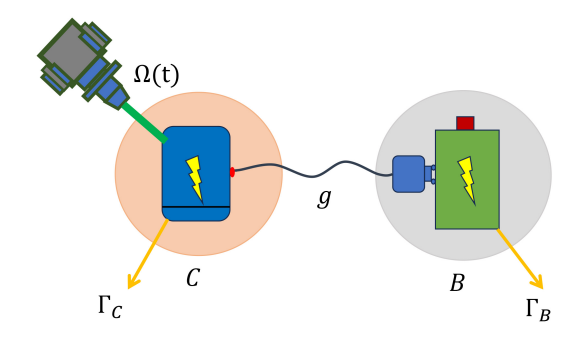


FIG. 1. The quantum battery model: Both the charger C and the quantum battery B are modeled as two-level systems and exposed to their respective dissipative environments. The corresponding transition frequencies are ω_C and ω_B , respectively. The direct coupling strength between the charger and the quantum battery is g. The charger is driven by an external field and subject to homodyne feedback control.

tum battery charging scheme that ensures stable battery charging while transforming finite temperatures into a favorable charging factor. The battery charging process is assisted by a charger which operates under homodyne quantum feedback control. This real-time feedback enables precise control of the quantum system, allowing more energy to be transferred into the battery. On the basis of this approach, we investigated the impact of bosonic and fermionic reservoirs with finite temperatures on the performance of quantum batteries. Unlike bosonic thermal reservoirs, fermionic reservoirs are typically modeled as two-level systems [101–106], with their components having discrete energy levels. Some studies are also exploring the potential advantages of using this type of reservoir [97, 98, 107–112].

In our proposal, we consider both the charger and the quantum battery to be modeled as two-level systems, each embedded in its respective environment; the remainder of the paper is organized as follows. In Sec. II, the charging model of the quantum battery is introduced and related physical quantities characterizing the performance of the quantum battery are provided, such as energy storage, maximum extractable energy, and charging efficiency of the battery. In Sec. III, the charging process of the quantum battery in bosonic and fermionic reservoirs is discussed. The results show that there exist optimal charging parameters, and a fermionic reservoir at a finite temperature is more conducive to enhancing the battery's performance. In Sec. IV, the single-particle quantum battery model is extended to a multi-particle quantum battery, and the impact of increasing the number of particles in the quantum battery on its performance is discussed. Finally, we give a summary of the present protocol in Sec. V.

II. DISSIPATIVE QUANTUM BATTERY MODEL

A. The model and the master equation of the system

We model the charger and the quantum battery as a two-level atom with an energy interval of $\omega_{\rm C}$ and $\omega_{\rm B}$ between the excited and ground states, respectively. Meanwhile, the charger and quantum battery are injected into their respective reservoirs, as shown in Fig. 1. Initially, the quantum battery is in the ground state $|g\rangle$. For convenience, we choose $\hbar=1$ in the whole paper, and we assume that the charger and quantum battery share the same transition frequency, that is, $\omega_{\rm C}=\omega_{\rm B}=\omega_0$. The total Hamiltonian of the system is $H=H_0+H_{\rm I}$, where

$$H_0 = \omega_0 \sigma_C^+ \sigma_C^- + \omega_0 \sigma_B^+ \sigma_B^- + \sum_k \omega_{Ck} a_k^{\dagger} a_k + \sum_k \omega_{Bk} b_k^{\dagger} b_k, \tag{1}$$

the first two terms represent the free Hamiltonian of the charger and the quantum battery, while the latter two terms correspond to the free Hamiltonian of the independent environments interacting with the charger and the battery, respectively. σ_j^+ and σ_j^- (j=C,B) are the raising and lowering operators for the corresponding systems. a_k^\dagger (a_k) , b_k^\dagger (b_k) , and ω_{jk} (j=C,B) are the creation (annihilation) operators and the frequency of the kth mode of the corresponding environments. In the interaction picture, the interacting Hamiltonian involved in the system is $H_{\rm I}=H_{\rm SI}+H_{\rm EI}$, where

$$H_{\rm SI} = g(\sigma_C^+ \sigma_B^- + \sigma_C^- \sigma_B^+), \tag{2}$$

$$H_{\text{EI}} = \sum_{k} g_{Ck} (\sigma_{C}^{+} a_{k} e^{i(\omega_{0} - \omega_{k})} + \sigma_{C}^{-} a_{k}^{\dagger} e^{-i(\omega_{0} - \omega_{k})})$$
$$+ \sum_{k} g_{Bk} (\sigma_{B}^{+} b_{k} e^{i(\omega_{0} - \omega_{k})} + \sigma_{B}^{-} b_{k}^{\dagger} e^{-i(\omega_{0} - \omega_{k})}) (3)$$

where g stands for the coupling strength between the charger and the quantum battery, and g_{jk} (j=C,B) is the coupling strength of the system with the respective kth mode environment. For simplicity, we assume $\omega_{Ck}=\omega_{Bk}=\omega_k$. During the charging process, a resonant drive is applied to the charger and then the charger resonates with the battery to exchange energy through the interaction. In the interaction picture and considering the rotating-wave approximation, the corresponding driving Hamiltonian is

$$H_{\text{drive}} = \Omega \sigma_C^y,$$
 (4)

where Ω is the strength of the drive field, which is usually constant in conventional schemes.

To improve the charging efficiency of the battery, a feed-back control is applied to the charger. The photons spontaneously emitted by the charger are collected and measured by a homodyne interferometer, thus obtaining the corresponding photocurrent represented by an appropriately normalized and shifted measurement record [113–115].

$$r(t)dt = \langle \sigma_C^x \rangle dt + \frac{dw(t)}{\sqrt{\eta \Gamma_C}}, \tag{5}$$

where $\langle \sigma_C^x \rangle$ stands for the corresponding expected value. dw(t) represents the Wiener increment, which satisfies $[dw(t)]^2 = dt$ and E[dw(t)] = 0. Γ_C is the spontaneous emission rate of the charger. η is the total measurement efficiency, which incorporates both the fraction of collected photons η_c and the detector efficiency η_d , so that $\eta = \eta_c \eta_d$. The feedback is achieved by applying a driving field that depends on the measured results. We consider the simplest case of direct feedback, where the drive strength is proportional to the measurement record, i.e.,

$$\Omega(t) = \Omega_0 - fr(t - \tau)dt, \tag{6}$$

where Ω_0 is a constant drive, which is set to zero here. f stands for the feedback strength, and τ expresses a small time delay in the feedback loop. Here, we consider the measurement efficiency to be $\eta=1$ and assume that the decay channel corresponding to photons collected by the detector remains at effectively zero temperature. Simultaneously, the quantum battery is considered to be in contact with a thermal reservoir at a finite temperature. In the Markovian limit of $\tau \to 0$ and weak coupling conditions [116–118], the evolution of the system based on feedback control can be determined by the following master equation [119]

$$\dot{\rho} = -i[H_{\rm SI}, \rho] + if[\sigma_C^y, \sigma_C^- \rho + \rho \sigma_C^+] + \frac{f^2}{\eta \Gamma_C} \mathcal{D}[\sigma_C^y] \rho + \mathcal{L}_C \rho + \mathcal{L}_B \rho. \tag{7}$$

The first term of Eq. (7) describes the coherent evolution introduced by the interaction between the charger and the quantum battery. The last two items in the first line describe the coherent evolution introduced by the feedback operation to the charger, and the measurement noise fed back to the system by the driver. The two terms in the second line describe the charger's spontaneous emission and the quantum battery's dissipation process, respectively.

The specific forms of $\mathcal{L}_{C}\rho$ and $\mathcal{L}_{B}\rho$ are as follows: $\mathcal{L}_C \rho = \Gamma_C [\sigma_C^- \rho \sigma_C^+ - 1/2(\sigma_C^+ \sigma_C^- \rho + \rho \sigma_C^+ \sigma_C^-)] \text{ and } \mathcal{L}_B \rho =$ $\gamma_B^{\downarrow}[\sigma_B^-\rho\sigma_B^+ - 1/2(\sigma_B^+\sigma_B^-\rho + \rho\sigma_B^+\sigma_B^-)] + \gamma_B^{\uparrow}[\sigma_B^+\rho\sigma_B^- - 1/2(\sigma_B^+\sigma_B^-\rho\sigma_B^-)]$ $1/2(\sigma_B^-\sigma_B^+\rho + \rho\sigma_B^-\sigma_B^+)$]. Here, we consider the case where the dynamics of the quantum battery is controlled by bosonic or fermionic thermal reservoirs, respectively. If the quantum battery interacts with a bosonic thermal reservoir, γ_B^{\downarrow} $\Gamma_B(1+n_b)$ and $\gamma_B^{\uparrow}=\Gamma_B n_b$, where Γ_B is the dissipation rate of the quantum battery and $n_b=1/(e^{1/T}-1)$ is the average excitation number of the corresponding thermal reservoir, in which T is the dimensionless temperature of the thermal reservoir. If the quantum battery interacts with a fermionic thermal reservoir, $\gamma_B^{\downarrow} = \Gamma_B(1 - n_f), \ \gamma_B^{\uparrow} = \Gamma_B n_f$ and $n_f = 1/(e^{1/T}+1)$. In the case of the fermionic thermal reservoir, it is easy to see that $0 < n_f < 1$, where $0 < n_f < 1/2$ $(1/2 < n_f < 1)$ means T > 0 (T < 0). Meanwhile, a negative temperature T < 0 can exhibit stationary states with population inversion [120–128]. Although the temperature of the fermionic thermal reservoir can be positive or negative, it is worth noting that the bosonic reservoir cannot attain negative temperatures, resulting in $0 < n_b < \infty$. In this work,

we limit the temperature of the fermionic thermal reservoir to the positive temperature range (T>0) to avoid population inversion induced by the thermal reservoir effects and then compare the effects of the fermionic thermal reservoir and the bosonic thermal reservoir on battery performance.

B. The related performance parameter of the quantum battery

At an arbitrary time t, the stored energy of the quantum battery is defined as

$$E_B(t) = \text{Tr}[H_B \rho_B(t)] - \text{Tr}[H_B \rho_B(0)], \tag{8}$$

where $H_B=\omega_0\sigma_B^+\sigma_B^-$, $\rho_B(t)=\mathrm{Tr}_C[\rho(t)]$ and $\rho_B(0)=|g\rangle_B\langle g|$ are the free Hamiltonian, the reduced density matrix and the initial state of the quantum battery, respectively. When the quantum battery is in the excited state $|e\rangle$, it means that it is fully charged, and the corresponding maximum stored energy is $E_B^{\mathrm{max}}=\omega_0$. To evaluate the useful work of the quantum battery storage, we use the concept of ergotropy [129, 130] and its form is as follows

$$\mathcal{E}(t) = \text{Tr}[H_B \rho_B(t)] - \min_{U} \text{Tr}[U \rho_B(t) U^{\dagger} H_B], \quad (9)$$

it describes the maximum energy that can be extracted from the battery. The second term in Eq. (9) indicates the minimum energy that cannot be extracted from the battery by executing all unitaries U in the system, and the state corresponding to the minimum energy is known as the passive state [131, 132].

The Hamiltonian H_B and the density matrix ρ_B of the quantum battery can be written in order using spectral decomposition as $H_B = \sum_j \varepsilon_j |\varepsilon_j\rangle \langle \varepsilon_j|$ $(\varepsilon_1 \leq \varepsilon_2 \cdots \leq \varepsilon_n)$, and $\rho_B = \sum_j r_j |r_j\rangle \langle r_j|$ $(r_1 \geq r_2 \cdots \geq r_n)$, respectively, the form of the passive state can be expressed as $\sigma = \sum_j r_j |\varepsilon_j\rangle \langle \varepsilon_j|$. Thus, the ergotropy can be rewritten as

$$\mathcal{E}(t) = \text{Tr}[H_B \rho_B(t)] - \text{Tr}[H_B \sigma]$$

= \text{Tr}[H_B \rho_B(t)] - \sum_i r_j \varepsilon_j. (10)

In addition to the stored energy and extractable energy of the quantum battery, the charging efficiency at steady state is another crucial performance metric. It is defined as the ratio of the maximum extractable energy to the stored energy, i.e.,

$$R = \frac{\mathcal{E}(\infty)}{E_B(\infty)}. (11)$$

The higher this ratio, the more useful work the battery can store, and the better its performance

III. THE CHARGING PROCESS OF A QUANTUM BATTERY IN DIFFERENT THERMAL RESERVOIR ENVIRONMENTS

A. The charging process of quantum battery in a bosonic thermal reservoir

In this part, we first consider the case where the quantum battery is in a bosonic thermal reservoir. After setting $\dot{\rho}=0$

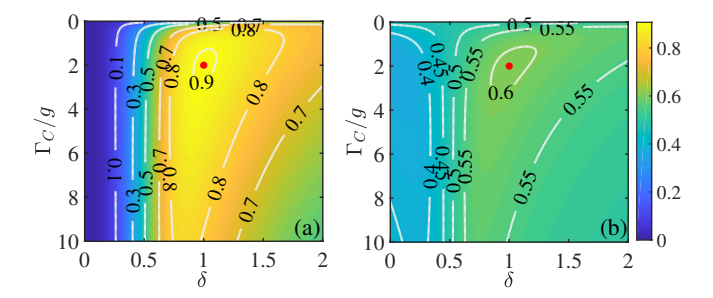


FIG. 2. Under a bosonic thermal reservoir, the stored energy of the quantum battery is a function of the feedback parameter δ and the dissipation rate Γ_C of the charger. The temperature of the bosonic thermal reservoir is T=0 ($n_b=0$) in (a), while in (b) the temperature of the bosonic thermal reservoir is $T=10~(n_b\approx 9.51)$. Solid red circles represent the optimal stored energy of the quantum battery, with the corresponding optimal charging parameters being $\Gamma_C=2g$ and $\delta=f/\Gamma_C=1$. Other parameters are $g=0.01\omega_0$ and $\Gamma_B = 0.1g$, respectively.

in Eq. (7), the steady-state solutions of the system are obtained (see Appendix A). Combined with Eq. (8), the stored energy of the battery is finally obtained as follows

$$E_B(\infty) = \omega_0 \frac{n_b W_b S + 4g^2 Q_b [2Q_b + \Gamma_C (1 - 2\delta)\eta + \Gamma_B \eta]}{(1 + 2n_b) W_b S + 4g^2 [2Q_b + \Gamma_C (1 - 2\delta)\eta + \Gamma_B \eta]}$$
(12)

where we set $\delta = f/\Gamma_C$, $S = 2\delta(\delta - \eta) + \eta$, $Q_b = \Gamma_C \delta^2 + n_b \Gamma_B \eta$ and $W_b = \Gamma_C \Gamma_B (\Gamma_C + \Gamma_B + 2n_b \Gamma_B)[4Q_b + 1]$ $(\Gamma_C + \Gamma_B - 4\Gamma_C \delta - 2n_b \Gamma_B)\eta$ for simplicity. See Appendix A for the corresponding calculation details. Under perfect measurement conditions ($\eta = 1$), we assume that the quantum battery is in an ideal closed state, which means that $\Gamma_B = 0$. At this time, the energy stored in the battery becomes

$$E_B(\infty) = \omega_0 \frac{\delta^2}{1 + 2(\delta - 1)\delta}.$$
 (13)

This clearly shows that when $\delta = f/\Gamma_C = 1$, the stored energy of the battery reaches its maximum value, that is, $E_B^{\rm max}(\infty) = \omega_0$. This implies that the effect of spontaneous emission on the charger can be offset by adjusting the feedback intensity f, enabling full charging of the quantum battery, this result is consistent with Ref. [80]. However, in practice, a quantum battery cannot be perfectly isolated from its surroundings, so it is necessary to consider placing it in an open system. To discuss the influence of feedback strength f and charger dissipation on quantum battery energy storage, we conduct corresponding numerical simulations according to Eq. (12) subsequently. In the absence of special instructions, the remaining parameters are set as follows: $\eta = 1$, $g = 0.01\omega_0$, and $\Gamma_B = 0.1g$.

Figures 2 (a) and (b) show the stored energy of the quantum battery as a function of the feedback parameter δ and the dissipation rate Γ_C of the charger when the battery is in a dissipative bosonic thermal reservoir with temperature T=0 $(n_b=0)$ and T=10 $(n_b\approx 9.51)$, respectively. The results show that the optimal stored energy of the battery is regulated by the feedback parameter δ and the dissipation rate Γ_C of the

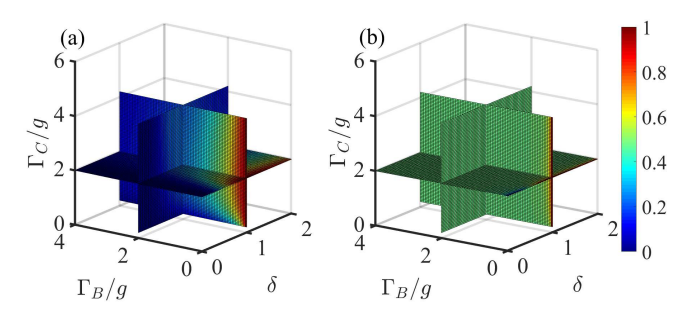


FIG. 3. The steady-state stored energy of the quantum battery is shown as a function of δ , Γ_B , and Γ_C . In panels (a) and (b), the temperature of the thermal reservoir is set to T = 0 and T = 10, respectively. The remaining parameters are the same as in Fig. 2.

charger, there exists a set of optimal parameters: $\Gamma_C = 2g$ and $\delta = f/\Gamma_C = 1$. Here, $\delta = 1$ means that the feedback strength f is equal to the dissipation rate Γ_C of the charger (i.e., $f = \Gamma_C$).

To determine whether optimal charging conditions are affected by the dissipation rate of the battery Γ_B , we explored the influence of the feedback parameter δ and the dissipation rate of the charger and the quantum battery on the stored en- $E_B(\infty) = \omega_0 \frac{n_b W_b S + 4g^2 Q_b [2Q_b + \Gamma_C (1-2\delta)\eta + \Gamma_B \eta]}{(1+2n_b)W_b S + 4g^2 [2Q_b + \Gamma_C (1-2\delta)\eta + \Gamma_B \eta]} \text{ thermal reservoir temperature for Figs. 3 (a) and (b) is } T = 0$ $(12) \qquad (n_b = 0) \text{ and } T = 10 \ (n_b \approx 9.51), \text{ respectively. The results}$ show that when the battery dissipation rate is zero ($\Gamma_B = 0$), there is no restriction on the magnitude of the dissipation rate Γ_C of the charger, as long as the optimal feedback parameter satisfies $\delta = f/\Gamma_C = 1$, the quantum battery can be fully charged. This is consistent with the results of the previous analysis. However, when the quantum battery is coupled to a dissipative environment, it can be observed that, under different battery dissipation rates, the stored energy of the quantum battery reaches its optimal value only when $\delta = 1$ and $\Gamma_C = 2g$. This demonstrates that the non-zero dissipation rate of the quantum battery does not affect its optimal charging conditions. In addition, when the temperature of the thermal reservoir and the dissipation rate of the battery are large, as shown in Fig. 3 (b), the stored energy of the battery does not change significantly with its dissipation rate.

> Under the perfect measurement ($\eta = 1$) and the optimal charging conditions ($\Gamma_C = 2g, \delta = 1$), the stored energy of the battery becomes

$$E_B^{\text{optimal}}(\infty) = \omega_0 \frac{4g^2 + 4gn_b\Gamma_B + n_b(1 + 2n_b)\Gamma_B^2}{(2g + \Gamma_B + 2n_b\Gamma_B)^2}.$$
 (14)

Based on Eq. (14), we explore the influence of quantum battery dissipation Γ_{B} on optimal steady-state energy storage at different temperatures in Fig. 4, where each curve corresponds to different temperatures. It can be seen that when the dissipation rate Γ_B of the battery is small, the optimal steady-state stored energy of the battery decreases with increasing temperature. When the dissipation rate Γ_B of the battery gradually increases, the optimal stored energy of the battery increases and approaches a constant value as the temperature increases. It is easy to see from Eq. (14) that when $\Gamma_B \gg g$ and $n_b \to \infty$

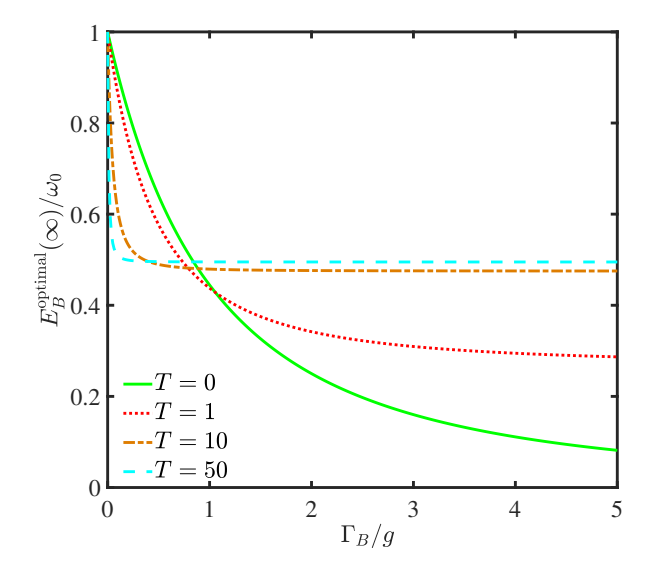


FIG. 4. Under optimal charging conditions ($\Gamma_C=2g,\delta=1$), the stored energy of the quantum battery in steady state varies with the battery dissipation rate. Different curves represent different temperatures of the bosonic thermal reservoir. The green solid line, red dotted line, yellow dash-dotted line, and blue dashed line correspond to the bosonic thermal reservoir temperature T of 0, 1, 10, and 50, respectively. The average thermal photon number as a function of temperature is given by $n_b=1/(e^{1/T}-1)$, where T=0 corresponds to $n_b=0$. All other parameters are the same as in Fig. 2.

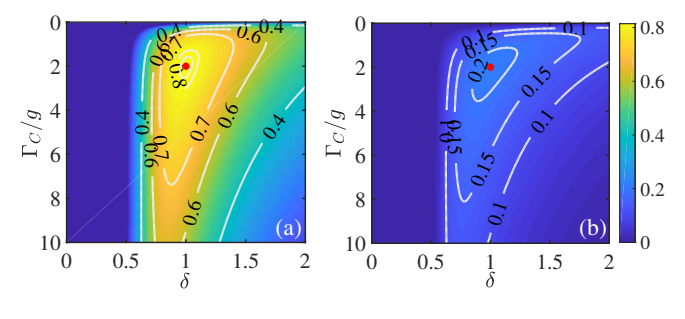


FIG. 5. The quantum battery is placed in a bosonic thermal reservoir: Panels (a) and (b) depict the ergotropy of the quantum battery as a function of the feedback parameter δ and the dissipation rate Γ_C of the charger in the steady state. The environmental temperatures corresponding to (a) and (b) are T=0 and T=10, respectively. Solid red circles represent the optimal ergotropy of the battery, with the corresponding optimal charging parameters being $\Gamma_C=2g$ and $\delta=f/\Gamma_C=1$. The other parameters are the same as in Fig. 2.

the battery stored energy $E_B^{\rm optimal}(\infty) \approx 0.5\omega_0$.

In addition to focusing on the stored energy of the quantum battery, the ergotropy of the quantum battery is also an important performance evaluation indicator. Similarly to Fig. 2, Fig. 5 plots the ergotropy of the quantum battery in the steady state as a function of the feedback parameter δ and the dissipation rate Γ_C of the charger, where the dissipation rate of the battery is $\Gamma_B=0.1g$. The results demonstrate that optimal charging parameters still exist for the battery ergotropy. These optimal conditions coincide with those for battery energy storage, namely $\Gamma_C=2g$ and $\delta=1$. As shown in Fig. 6,

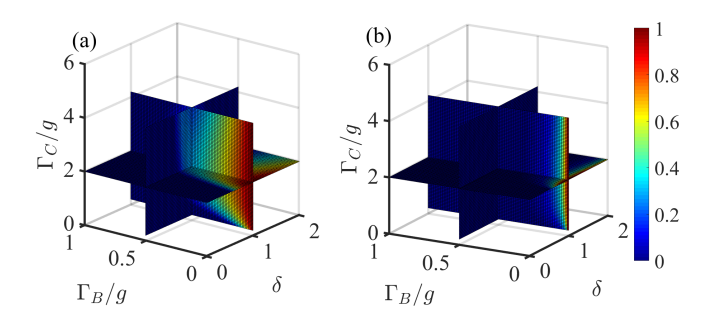


FIG. 6. Panels (a) and (b) show the steady-state ergotropy of the quantum battery as a function of δ , Γ_B , and Γ_C , with the thermal reservoir temperatures set to T=0 and T=10, respectively. The remaining parameters are identical to those in Fig. 2.

the optimal charging conditions for the ergotropy of the quantum battery also remain independent of the dissipation rate of the battery Γ_B . Furthermore, when the dissipation rate Γ_B of the quantum battery increases to a certain value, the ergotropy of the battery is zero regardless of the value of Γ_C and δ . This indicates that no energy can be extracted from the battery, and the feedback control mechanism becomes ineffective.

Under the optimal charging parameters ($\Gamma_C=2g,\delta=f/\Gamma_C=1$), the maximum extractable energy (the ergotropy) of the quantum battery in the bosonic thermal reservoir is

$$\mathcal{E}(\infty) = \omega_0 \left[\frac{8g^2(1+n_b) + (1+2n_b)|\beta_b|}{2(1+2n_b)(2g+\Gamma_B+2n_b\Gamma_B)^2} - \frac{1}{2(1+2n_b)} \right],$$
(15)

where $\beta_b = -4g^2 + 4g\Gamma_B + (1 + 2n_b)\Gamma_B^2$. Here, β_b can be positive or negative; therefore, we will discuss the cases separately. When $\beta_b \geq 0$, the ergotropy of the battery becomes $\mathcal{E}(\infty) = 0$, indicating that no energy can be extracted from the battery. According to the condition of $\beta_b = 0$, we can also determine that the critical value of the battery dissipation rate Γ_B at different temperatures is $\Gamma_B/g=2\left(-1+\sqrt{2}\sqrt{1+n_b}\right)/(1+2n_b)$. When the dissipation rate of the battery Γ_B exceeds this critical value, no energy can be extracted from the battery. Furthermore, the result shows that this critical value decreases monotonically with increasing temperature. Under high-temperature conditions, the quantum battery must maintain a sufficiently low dissipation rate to ensure the viability of the charging protocol; otherwise, the protocol fails. These results highlight the fundamental limitations that temperature imposes on the quantum battery charging protocol. When $\beta_b < 0$, the ergotropy of the quantum battery becomes

$$\mathcal{E}(\infty) = \omega_0 \frac{4g^2 - 4g\Gamma_B - (1 + 2n_b)\Gamma_B^2}{(2g + \Gamma_B + 2n_b\Gamma_B)^2}.$$
 (16)

The result indicates that as the temperature increases, the extractable energy of the battery gradually decreases. In general, when the battery is in a bosonic thermal reservoir, the temperature not only narrows the permissible range of the dissipation rate of the battery but also reduces its extractable energy.

Subsequently, to more intuitively illustrate the impact of temperature and battery dissipation rate on the ergotropy of

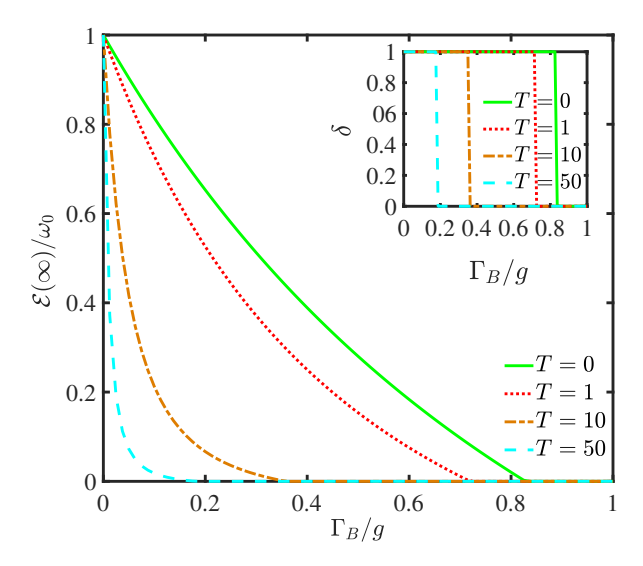


FIG. 7. The ergotropy of the quantum battery in the steady state is shown as a function of the battery dissipation rate Γ_B , where the dissipation rate of the charger is fixed at its optimal value, i.e., $\Gamma_C=2g$. The corresponding optimal feedback parameter δ is shown in the inset. Different curves correspond to different thermal reservoir temperatures. The green solid line, red dotted line, yellow dash-dotted line, and blue dashed line correspond to the bosonic thermal reservoir temperature T of 0, 1, 10, and 50, respectively. The remaining parameters are the same as in Fig. 2.

the quantum battery, we further analyze how the ergotropy of the quantum battery varies with the dissipation rate Γ_B of the battery at different temperatures, as shown in Fig. 7, where the dissipation rate of the charger is set to the optimal value $\Gamma_C = 2g$. The corresponding optimal feedback parameters δ are also shown in the inset. The results show that when the temperature of the thermal reservoir is constant, the ergotropy gradually decreases with increasing dissipation rate Γ_B . At the same time, the dissipation rate Γ_B of the battery has a critical value. If Γ_B exceeds this threshold, the battery extraction energy becomes zero. In addition, this critical value decreases as the temperature increases. The inset shows that if Γ_B does not exceed this critical value, the corresponding optimal feedback parameter remains $\delta = 1$. Furthermore, it can be observed that increasing the temperature is not conducive to extracting energy from the battery.

To evaluate the influence of the environment of the bosonic thermal reservoir on the battery charging efficiency R, we explored the impact of the temperature of the bosonic thermal reservoir on the quantum battery charging efficiency under optimal charging conditions ($\Gamma_C=2g,\delta=1$), as shown in Fig. 8, with $\Gamma_B=0.1g$. The definition of battery charging efficiency is given in Eq. (11). The results show that the charging efficiency R of the quantum battery decreases with increasing temperature T, which means that the increase in the temperature of the reservoir inhibits the efficiency of energy extraction from the battery.

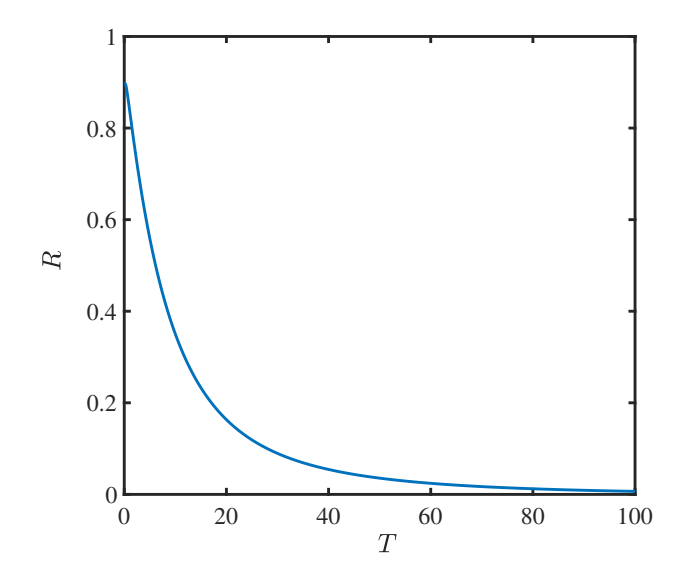


FIG. 8. Under the optimal charging conditions in a bosonic thermal reservoir, the charging efficiency R of the quantum battery is shown as a function of temperature T, with $\Gamma_B=0.1g$.

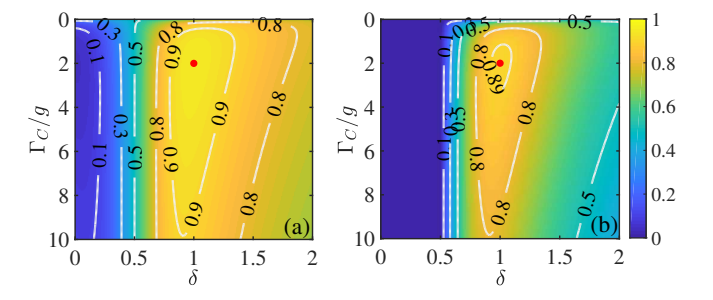


FIG. 9. The quantum battery is placed in a fermionic reservoir: Panels (a) and (b) describe steady-state stored energy and the ergotropy of the quantum battery as a function of the feedback parameter δ and the dissipation rate Γ_C of the charger, respectively. The temperature of the fermionic reservoir is T=10, the other parameters are the same as in Fig. 2.

B. The charging process of quantum battery in fermionic thermal reservoir

Next, we consider the scenario in which the quantum battery is embedded in a finite-temperature fermionic thermal reservoir. By solving Eq. (7), we obtain that the stored energy of the quantum battery is given by

$$E_B(\infty) = \omega_0 \frac{4g^2 Q_f (\Gamma_B \eta + \Gamma_C S) + n_f W_f S}{4g^2 (\Gamma_B \eta + \Gamma_C S)^2 + W_f S}, \quad (17)$$

where we set $\delta = f/\Gamma_C$, $S = 2\delta(\delta - \eta) + \eta$, $Q_f = \Gamma_C \delta^2 + n_f \Gamma_B \eta$ and $W_f = \Gamma_C \Gamma_B (\Gamma_C + \Gamma_B) [\Gamma_B \eta + \Gamma_C (2S - \eta)]$.

For a zero-temperature thermal reservoir, the average excitation number of the thermal reservoir satisfies $n_{b(f)}=0$. As Eq. (7) shows, the master equation governing the dynamics of the control system has the same form for both bosonic and fermionic thermal reservoirs. Therefore, we will not specifically consider the scenario in which the temperature of the

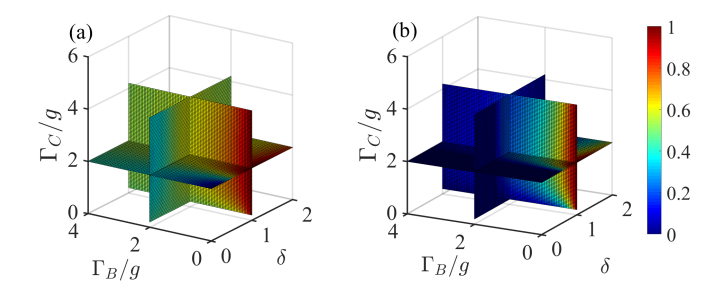


FIG. 10. Panels (a) and (b) show the steady-state stored energy and ergotropy of the quantum battery, respectively, as functions of δ , Γ_B , and Γ_C . The fermionic reservoir temperature is set to T=10. All other parameters are the same as in Fig. 2.

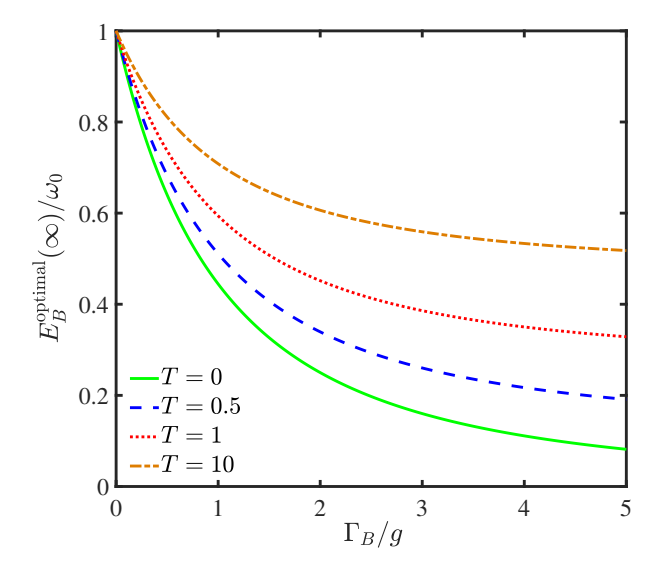


FIG. 11. Under optimal charging conditions ($\Gamma_C=2g,\delta=1$), the steady-state stored energy of the quantum battery is shown as a function of the battery dissipation rate. Different curves correspond to different reservoir temperatures. The green solid line, blue dashed line, red dotted line, and yellow dash-dotted line correspond to the fermionic thermal reservoir temperature T of 0, 0.5, 1, and 10, respectively. The average thermal excitation number follows $n_f=1/(e^{1/T}+1)$, where T=0 corresponds to $n_f=0$. Other parameters match those in Fig. 2.

fermionic thermal reservoir is T=0. Figures 9 (a) and 9 (b) show the steady-state dependence of the battery's stored energy and ergotropy on the feedback parameter δ and the charger dissipation rate Γ_C , respectively. Here, the temperature of the thermal reservoir is set at T=10 and the dissipation rate of the battery is set at $\Gamma_B=0.1g$. The results reveal the existence of optimal charging parameters that simultaneously maximize both the stored energy and the ergotropy of the quantum battery, which coincide with those obtained for the bosonic reservoir case. Furthermore, Fig. 10 again confirms that these parameters remain independent of the battery dissipation rate Γ_B .

Under the perfect measurement ($\eta=1$) and the optimal charging conditions ($\Gamma_C=2g,\,\delta=1$), the stored energy of

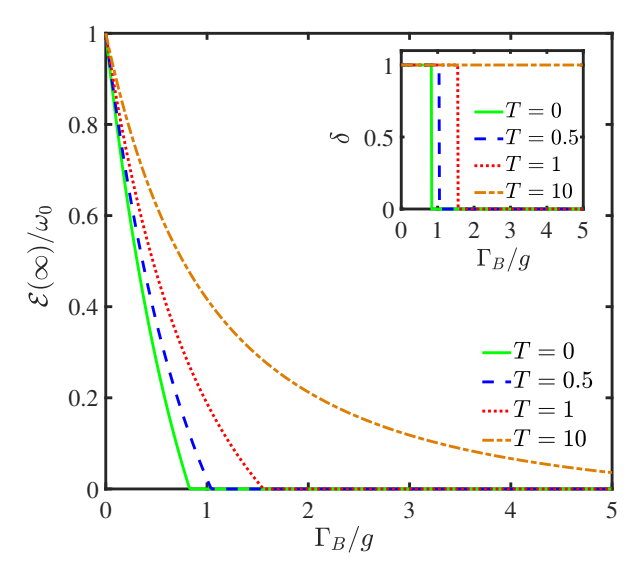


FIG. 12. The steady-state ergotropy of the quantum battery is shown as a function of Γ_B , with different curves corresponding to different fermionic thermal reservoir temperatures. The dissipation rate of the charger is set to $\Gamma_C=2g$, and the corresponding optimal feedback parameters δ are shown in the inset.

the battery becomes

$$E_B^{\text{optimal}}(\infty) = \omega_0 \frac{4g^2 + n_f(\Gamma_B^2 + 4g\Gamma_B)}{(2g + \Gamma_B)^2}.$$
 (18)

As shown in Eq. (18), for a fixed dissipation rate Γ_B , the stored energy of the quantum battery increases monotonically with temperature. The corresponding numerical results appear in Fig. 11, with distinct curves corresponding to different reservoir temperatures. In contrast to the bosonic reservoir case, elevated temperatures consistently enhance the battery energy storage capacity, regardless of the magnitude of the dissipation rate Γ_B of the battery.

Under optimal charging parameters ($\Gamma_C=2g,\,\delta=1$), the maximum extractable energy (the ergotropy) of the quantum battery can be expressed as:

$$\mathcal{E}(\infty) = \omega_0 \frac{\beta_f + |\beta_f|}{(2q + \Gamma_B)^2},\tag{19}$$

where $\beta_f=4g^2+4g(-1+2n_f)\Gamma_B+(-1+2n_f)\Gamma_B^2$. We analyze the problem in two scenarios. First, when $\beta_f\leq 0$, we obtain $\mathcal{E}(\infty)=0$, which means that energy cannot be extracted from the quantum battery. Setting $\beta_f=0$, we derive the critical battery dissipation rate in the positive temperature regime as $\Gamma_B/g=2/(1-2n_f+\sqrt{4n_f^2-6n_f+2})$, which is a temperature-dependent function. Once Γ_B exceeds the critical value, the battery can no longer supply energy to other devices. On the basis of the critical condition analysis, we observe that as the temperature increases, the permissible range

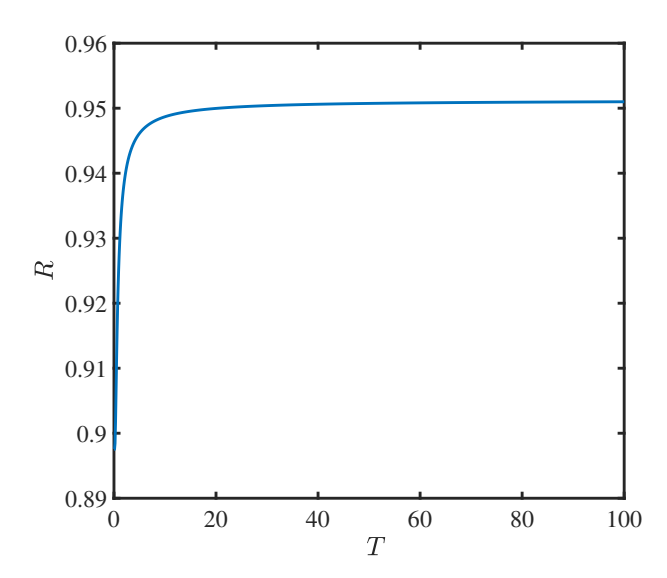


FIG. 13. Under the optimal charging conditions of the fermionic thermal reservoir, the charging efficiency R of the quantum battery is a function of the temperature T, with $\Gamma_B=0.1g$.

of the battery dissipation rate broadens. When $\beta_f > 0$, then

$$\mathcal{E}(\infty) = \omega_0 \frac{2\beta_f}{(2g + \Gamma_B)^2} = \omega_0 \left[\frac{8g\Gamma_B + 2\Gamma_B^2}{(2g + \Gamma_B)^2} n_f + (4g^2 - 4g\Gamma_B - \Gamma_B^2) \right] (20)$$

The above equation indicates that, for fixed g and Γ_B , the extractable energy from the quantum battery increases with temperature. In summary, when the quantum battery is coupled to a fermionic thermal reservoir, higher temperatures not only broaden the permissible range of the battery's dissipation rate but also enhance the battery's energy extraction capability.

Figure 12 illustrates the dependence of the quantum battery ergotropy on its dissipation rate, where the dissipation rate of the charger remains at its optimal value ($\Gamma_C = 2g$). The corresponding optimal feedback parameters are presented in the inset. The results demonstrate that increasing temperature promotes the extraction of battery energy. Similarly to the bosonic thermal reservoir case, there exists a critical value for the dissipation rate Γ_B of the battery in terms of energy extraction. In particular, when the battery is coupled to a fermionic thermal reservoir, an increase in temperature extends the critical point of the dissipation rate of the battery Γ_B and improves its usability. Subsequently, we explore the influence of the temperature of the fermionic thermal reservoir on the charging efficiency R of the battery under optimal charging conditions through Fig. 13, where the dissipation rate of the battery is $\Gamma_B = 0.1q$. The results show that the charging efficiency R increases with temperature, suggesting that the temperature can serve as a resource to improve battery performance. This is different from the scheme proposed in reference [97], which exhibits the temperature will be unfavorable for the extraction of battery energy, when the environment is within the positive

temperature range, while in our scheme, temperature is still a favorable factor for battery charging. We have conducted a simple comparative analysis of these two schemes in the Appendix B.

IV. MULTIPARTICLE QUANTUM BATTERY MODEL

On the basis of the quantum feedback mechanism, we extend the previously proposed single-particle battery model to a multi-particle configuration. In this extended model, the charger consists of a single two-level atom embedded in a zero-temperature reservoir. During the charging process, quantum feedback control is applied to the charger. The quantum battery is composed of multiple two-level atoms and is embedded in a common thermal reservoir. The coupling strength between the charger and each atom in the battery is g. The free Hamiltonian form of the multi-particle quantum battery is given by form

$$H_B = \frac{\omega_0}{2} \sum_{i=1}^{N} \sigma_{iB}^z = \omega_0 S_B^z,$$
 (21)

where $S_B^{x,y,z} = \sum_i \sigma_{iB}^{x,y,z}/2$ denotes the collective atom operators of the quantum battery and N denotes the number of atoms comprising the battery.

In the Markovian limit (i.e., $\tau \to 0$), the evolution of the system is described by the following master equation

$$\dot{\rho} = -i[H'_{SI}, \rho] + if[\sigma_C^y, \sigma_C^- \rho + \rho \sigma_C^+] + \frac{f^2}{\eta \Gamma_C} \mathcal{D}[\sigma_C^y] \rho + \mathcal{L}_C \rho + \mathcal{L}_B' \rho.$$
(22)

At this point, the interaction term H'_{SI} between the charger and the quantum battery, as well as the Lindblad term $\mathcal{L}'_B \rho$ for the quantum battery, is given by the following forms

$$H'_{SI} = \sum_{i=1}^{N} g_i (\sigma_C^+ \sigma_{iB}^- + \sigma_C^- \sigma_{iB}^+) + \sum_{i < j}^{N} J_i (\sigma_{iB}^+ \sigma_{jB}^- + \sigma_{iB}^- \sigma_{jB}^+),$$
(23)

$$\mathcal{L}'_{B}\rho = \gamma_{B}^{\downarrow} [L_{B}^{-}\rho L_{B}^{+} - 1/2(L_{B}^{+}L_{B}^{-}\rho + \rho L_{B}^{+}L_{B}^{-})] + \gamma_{B}^{\uparrow} [L_{B}^{+}\rho L_{B}^{-} - 1/2(L_{B}^{-}L_{B}^{+}\rho + \rho L_{B}^{-}L_{B}^{+})], (24)$$

the first term of Eq. (23) describes the direct coupling between the charger and the constituent atoms of the quantum battery, while the second term accounts for the interactions between the atoms within the battery itself. For simplicity, we assume $g_i = g$ and $J_i = J$. In Eq. (24), $L_B^- = \sum_{i=1}^N \sigma_{iB}^-$ denotes the collective lowering operator of the quantum battery. To facilitate a fair comparison with the single-particle quantum battery, the steady state energy density of the multi-particle quantum battery is defined as follows

$$W = \frac{E_B(\infty)}{N} = \omega_0 \left(\frac{\langle S_B^z(\infty) \rangle}{N} + \frac{1}{2} \right), \quad (25)$$

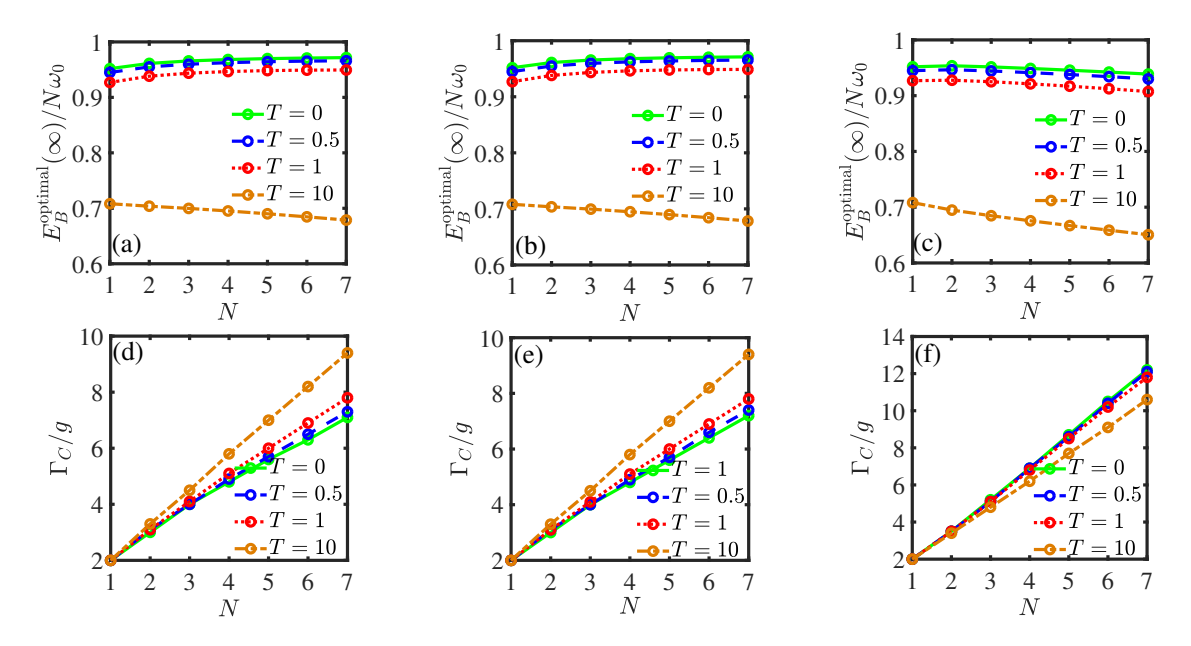


FIG. 14. The multi-particle quantum battery is placed in a bosonic thermal reservoir, its optimal energy storage is analyzed as a function of the number of constituent quantum battery particles at different reservoir temperatures. The coupling strengths between the internal particles of the quantum battery in panels (a), (b), and (c) are J=0, J=0.1g, and J=g, respectively. The corresponding optimal charger dissipation parameters Γ_C are shown in panels (d), (e), and (f). The remaining parameters are set as $g=0.01\omega_0$, $\delta=f/\Gamma_C=1$, and $\Gamma_B=0.05g$.

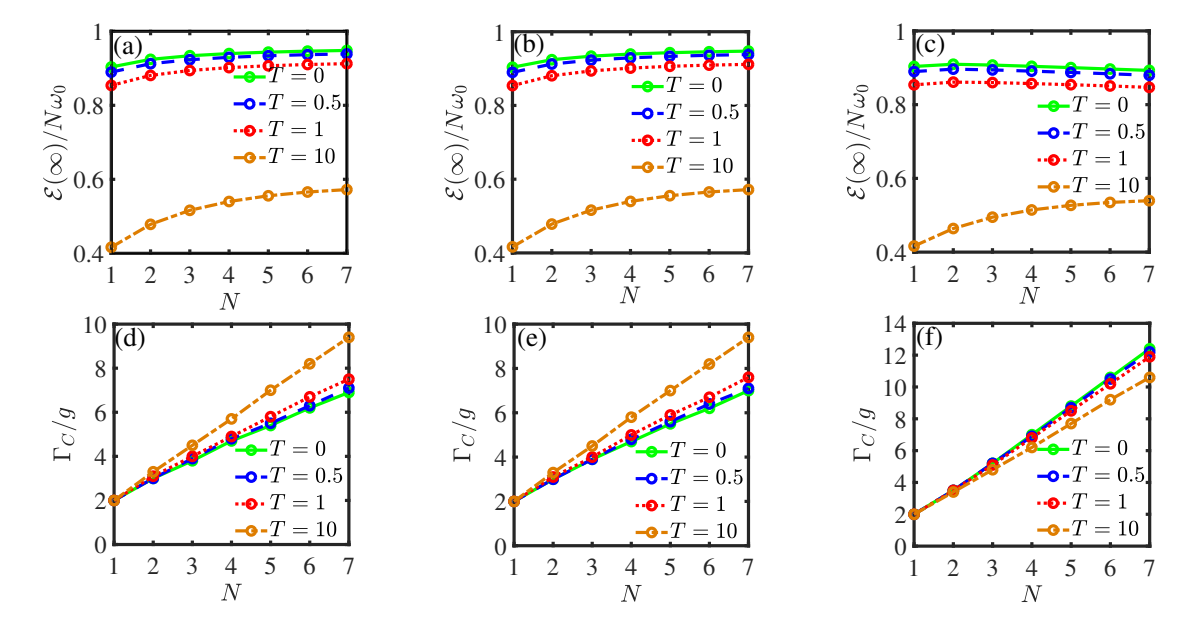


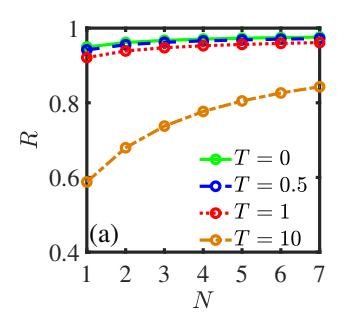
FIG. 15. In the bosonic thermal reservoir, panels (a)-(c) depict the variation of the average ergotropy of the quantum battery in the steady state as a function of the particle number N, with the corresponding atom-atom coupling strengths in the multi-particle quantum battery set to J=0, J=0.1g, and J=g, respectively. Panels (d)-(f) represent the optimal dissipation rate Γ_C of the charger corresponding to panels (a)-(c). Different curves represent different temperatures, while the other parameters are identical to those in Fig. 14.

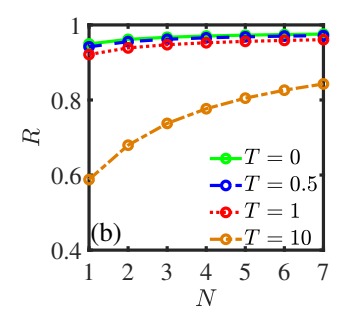
thus, the steady-state stored energy of the battery is

$$E_B(\infty) = NW. \tag{26}$$

In the following, we investigate the performance of the multi-particle quantum battery under different thermal reservoirs. The feedback parameter is set to $\delta=f/\Gamma_C=1$ to fa-

cilitate a more meaningful comparison with the single-particle quantum battery in the subsequent analysis.





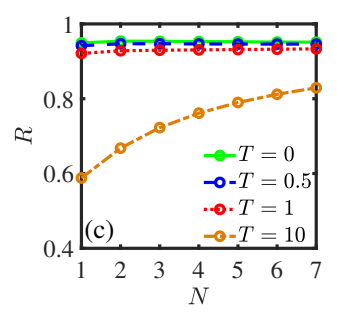


FIG. 16. The multi-particle quantum battery is placed in a bosonic thermal reservoir. The charging efficiency R of the battery is analyzed as a function of the number of particles N. The interparticle interaction strengths of the multi-particle quantum battery in panels (a)-(c) are set to J=0,J=0.1g, and J=g, respectively. Different curves represent different temperatures, while all other parameters are identical to those in Fig. 14.

A. The charging process of the multi-particle quantum battery in a bosonic thermal reservoir

First, we investigate the charging process of the multiparticle quantum battery in a bosonic thermal reservoir, in this case, $\gamma_B^{\downarrow} = \Gamma_B(1+n_b)$ and $\gamma_B^{\uparrow} = \Gamma_B n_b$ in Eq. (24). To explore the effects of the number of quantum battery particles Nand the interparticle interactions J on battery performance, we examine the optimal energy density of the battery as a function of N under three coupling regimes: no coupling (J=0), weak coupling (J = 0.1g) and strong coupling (J = g), as shown in Figs. 14 (a)-(c). The quantum battery operates in the desired weak dissipation regime with $\Gamma_B = 0.05g$, and the different curves correspond to different thermal reservoir temperatures. Additionally, the corresponding optimal charger dissipation rates for Figs. 14 (a)-(c) are presented in Figs. 14 (d)-(f). The results indicate that, similar to the singleparticle quantum battery case, temperature remains a detrimental factor for charging. Furthermore, it is observed that, under low-temperature conditions, the energy density of the battery increases with the number of particles when the interparticle couplings are absent or weak, as shown in Fig. 14 (a) and Fig. 14 (b). However, at higher temperatures, the energy density decreases as particle number increases, thus impairing efficient energy transfer to the battery. Furthermore, in the strong interparticle coupling regime, both elevated temperature and an increased number of particles have detrimental effects on the energy storage capacity of the battery, as illustrated in Fig. 14(c).

Subsequently, Fig. 15 presents the dependence of the maximum extractable energy per particle (i.e., the average ergotropy) of the multi-particle quantum battery on the number of particles N. As shown in Figs. 15 (a)-(b), when there is no interparticle interaction (J=0) or the interaction is weak (J=0.1g), the average ergotropy of the battery increases as the number of particles N increases. Meanwhile, when the number of particles in a multi-particle quantum battery is fixed, the average ergotropy decreases as the temperature increases, which means that temperature inhibits the extraction of energy from the battery. In addition, when the interaction between particles in a multi-particle quantum battery is strong

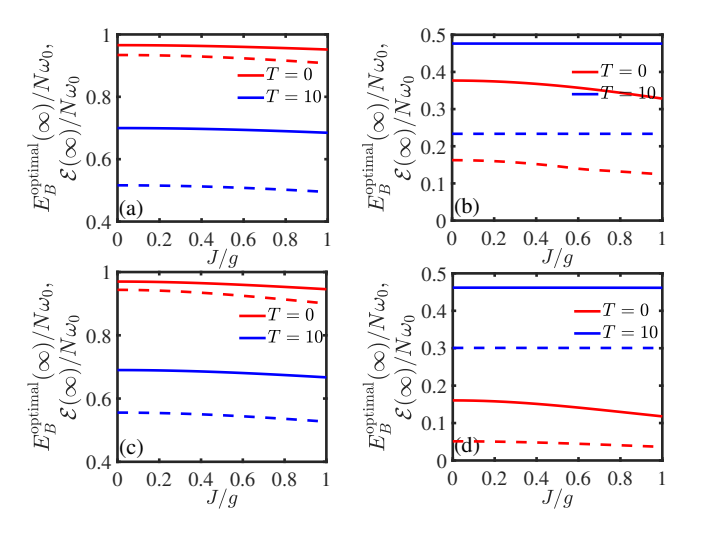


FIG. 17. The multi-particle quantum battery is placed in a bosonic thermal reservoir. The solid line represents the energy density of the multi-particle quantum battery, while the dashed line represents the maximum extractable energy per particle (average ergotropy). Curves of different colors correspond to different temperatures, with the red curve representing T=0 ($n_b=0$) and the blue curve representing T=10 [$n_b=1/(e^{1/10}-1)\approx 9.51$]. Panels (a) and (b) correspond to 3-particle quantum batteries with dissipation rates $\Gamma_B=0.05g$ and $\Gamma_B=0.5g$, respectively, while Panels (c) and (d) correspond to 5-particle quantum batteries with the same dissipation rates. All other parameters are identical to those in Fig. 14.

(J=g), the average ergotropy of the battery exhibits a slight decrease with increasing particle number N at low temperatures. In contrast, at high temperatures, this behavior is suppressed, and the average ergotropy increases as the number of particles N increases, but remains lower than that observed at low temperatures. As seen in Figs. 14 (d)-(f) and Figs. 15 (d)-(f), both in terms of energy storage and energy extraction, the optimal dissipation rate of the charger required increases with the number of particles. Figure 16 investigates the effects of temperature and particle number N on the charging efficiency R of the battery. Panels (a)-(c) correspond to J=0, J=0.1g, and J=g, respectively, and the different curves represent different temperatures of the thermal reservoir. It is

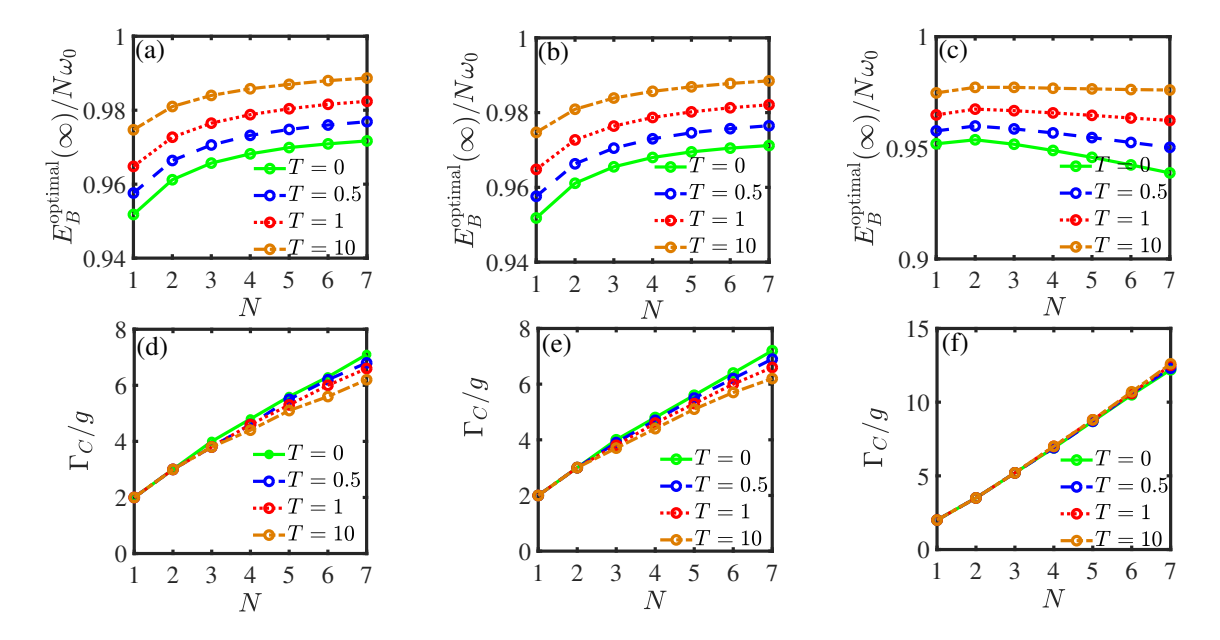


FIG. 18. The multi-particle quantum battery is placed in a fermionic thermal reservoir. Panels (a)-(c) depict the variation in the steady-state energy density of the multi-particle quantum battery as a function of particle number N for J=0, J=0.1g, and J=g, respectively. Panels (d)-(f) correspond to the optimal charger dissipation parameters required for Panels (a)-(c). Different curves correspond to different temperatures. The other parameters are the same as those in Fig. 14.

observed that at high temperatures, the charging efficiency ${\cal R}$ is more significantly affected by the number of battery particles, whereas this influence is greatly reduced at low temperatures. Overall, temperature remains a detrimental factor for both energy storage and extraction in the multi-particle quantum battery. However, there exist two specific scenarios in which an increase in the number of quantum battery particles can be beneficial for energy extraction: one occurs with weak interparticle interactions, and the other at high temperatures with strong interparticle interactions. The multi-particle quantum battery operates in a strong dissipation regime, as discussed in the Appendix ${\bf C}$.

In the following, we further investigate the effect of interparticle interaction strength J on the energy density and the average ergotropy of multi-particle quantum batteries by analyzing the cases of three-particle and five-particle quantum batteries. Figure 17 plots the variation of the energy density (solid lines) and the average ergotropy (dashed lines) with interparticle interaction J at different temperatures and the dissipation rates of the battery Γ_B . Specifically, Figs. 17 (a)-(b) correspond to the case of the 3-particle quantum battery, with dissipation rates of $\Gamma_B = 0.05g$ and $\Gamma_B = 0.5g$, respectively. Figures 17 (c)-(d) correspond to the case of the 5-particle quantum battery. The curves in different colors represent different temperatures of the bosonic thermal reservoir, with the red curve corresponding to T=0 and the blue curve corresponding to T=10. The results indicate that, regardless of whether the quantum battery operates under a weak or strong dissipation regime, interparticle interactions tend to degrade the performance of the multi-particle quantum battery. Compared to the weak dissipation regime, strong dissipation significantly impairs the energy storage and extraction capabilities of the quantum battery. However, under a strong dissipation regime, a high-temperature environment can enhance both energy storage and extraction.

B. The charging process of the multi-particle quantum battery in a fermionic thermal reservoir

Next, we investigate the charging process of the multiparticle quantum battery coupled to a fermionic thermal reservoir. In this scenario, $\gamma_B^{\downarrow} = \Gamma_B(1-n_f)$ and $\gamma_B^{\uparrow} = \Gamma_B n_f$ in Eq. (24).

Firstly, we explore the effects of a finite-temperature fermionic thermal reservoir on the energy storage and maximum extractable energy (ergotropy) of the multi-particle quantum battery, under the weak dissipation condition ($\Gamma_B=0.05g$). Furthermore, we examine the effects of the interparticle interaction strength J and the number of particles N on the battery performance, aiming to identify a more efficient charging mechanism.

Figures 18 (a)-(c) respectively illustrate the variation of energy density (i.e., the stored energy per particle) of the multiparticle quantum battery as a function of the number of particles N, under three different conditions: no coupling (J=0), weak coupling (J=0.1g), and strong coupling (J=g) between the internal particles of the battery. The optimal charger dissipation rates corresponding to Figs. 18 (a)-(c) are presented in Figs. 18 (d)-(f). The numerical results show that when the interaction strength J between particles is relatively weak (J=0 or 0.1g), increasing the number of battery particles enhances the energy density of the multi-particle quantum battery. Moreover, a higher temperature also leads to an in-

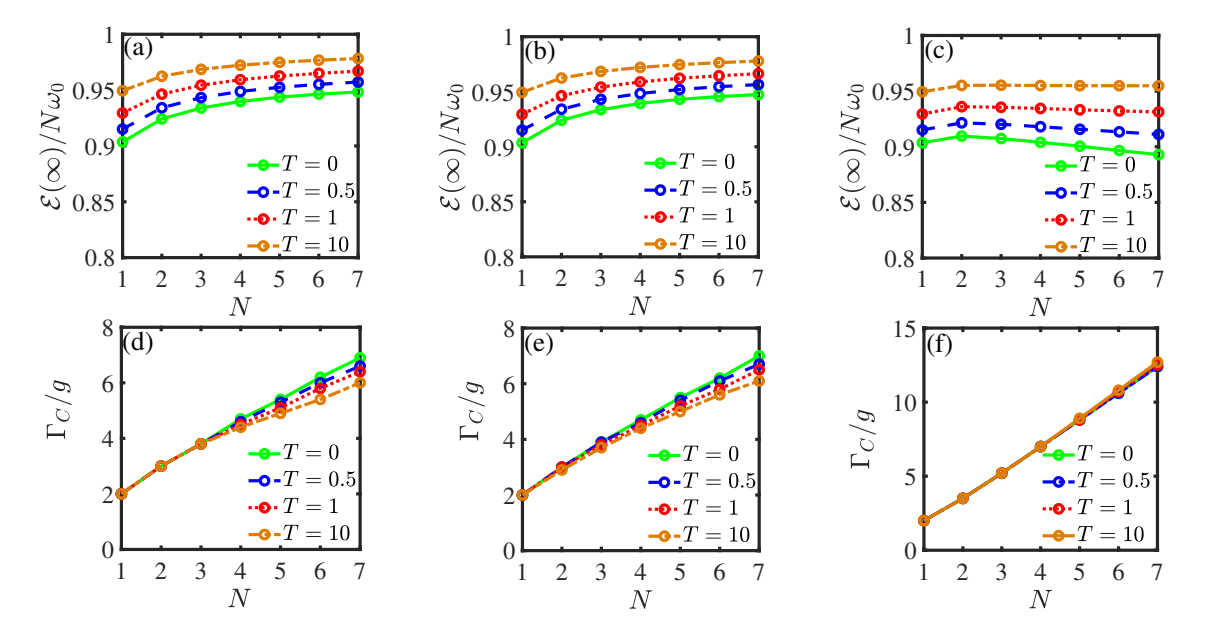


FIG. 19. The multi-particle quantum battery is embedded in a fermionic thermal reservoir. The average ergotropy of the multi-particle quantum battery is plotted as a function of the number of particles N, with all other parameters consistent with those in Fig. 14.

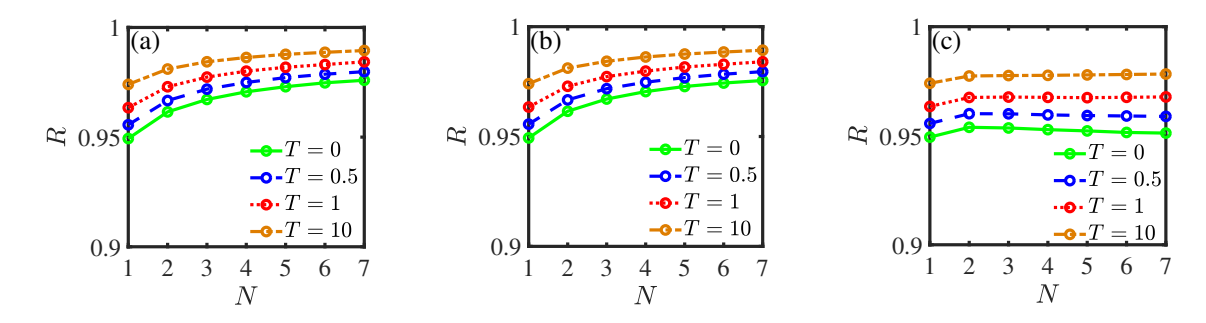


FIG. 20. Panels (a)-(c) respectively depict the variation in the charging efficiency R of the multi-particle quantum battery in the steady state with the number of particles N in a fermionic thermal reservoir. The other parameters are the same as those in Fig. 14.

crease in energy density. Similar to the single-particle battery case, temperature remains a favorable factor in the charging process. In the case of a relatively strong interaction strength J, it can be observed from Fig. 18 (c) that the energy density of the multi-particle quantum battery decreases as the number of particles N increases under low temperature conditions. As the temperature increases, the impact of the number of particles on energy storage becomes less pronounced. Furthermore, Figs. 18 (d)-(f) indicate that the optimal dissipation rate Γ_C of the charger required to maximize energy storage increases with the number of battery particles N increases.

Figure 19 illustrates the impact of the reservoir temperature, particle number N, and the interparticle interaction J on the average ergotropy of the multi-particle quantum battery in a finite-temperature fermionic thermal reservoir. The results indicate that the behavior of the ergotropy closely resembles that of the energy storage in the battery. Figure 20 reveals the influences of the temperature and the particle number N on the charging efficiency R of the multi-particle quantum battery. First, it can be observed that an increase in temperature

enhances the charging efficiency R of the multi-particle quantum battery. Second, when the interparticle coupling strength is weak (J=0 or 0.1g), R increases as the particle number N increases. However, when the interparticle coupling strength J is strong (J=g), an increase in N leads to a reduction in the charging efficiency R at low temperatures. In contrast, at high temperatures, the effect of increasing particle number on the charging efficiency becomes less pronounced. Based on the above research findings, we observe that when the dissipation rate of the multi-particle quantum battery in a fermionic thermal reservoir is weak, higher temperatures and weaker interparticle coupling enhance the performance of the quantum battery. The case of a strongly dissipative quantum battery is discussed in the Appendix D.

Subsequently, we continue to examine the impact of interparticle interaction J on both the energy density and average ergotropy of the multi-particle quantum battery, using 3-particle and 5-particle quantum batteries as representative cases, as shown in Fig. 21. Panels (a)-(b) display the numerical results for the three-particle quantum battery with dissi-

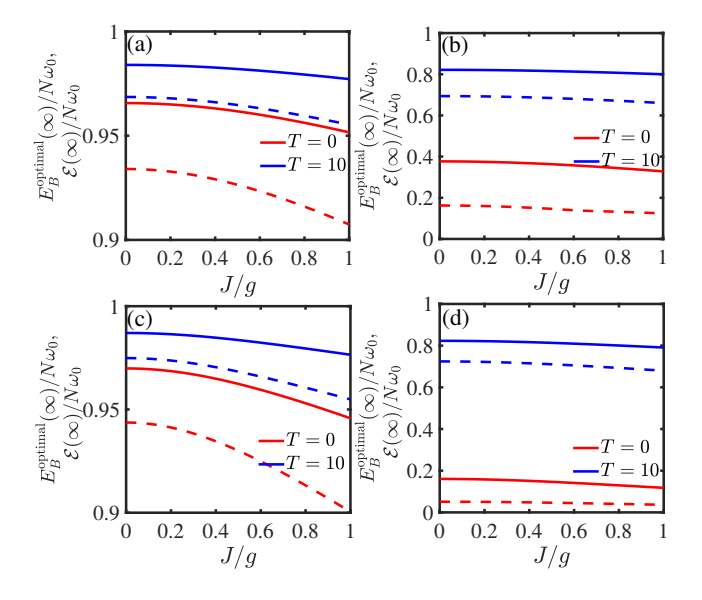


FIG. 21. Similar to Fig. 17, panels (a)-(b) and (c)-(d) respectively show the variations in the energy density and the average ergotropy for the 3-particle and 5-particle quantum batteries under weak dissipation rate $\Gamma_B=0.05g$ and strong dissipation rate $\Gamma_B=0.5g$, as functions of the interparticle coupling strength J of the battery. The red curve corresponds to T=0 ($n_f=0$) and the blue curve corresponds to T=10 [$n_f=1/(e^{1/10}+1)\approx 0.475$].

pation rates $\Gamma_B=0.05g$ and $\Gamma_B=0.5g$, respectively, while panels (c)-(d) show the results for corresponding five-particle quantum battery under identical dissipation conditions. The red and blue curves correspond to the fermionic thermal reservoir temperatures of the T=0 and T=10, respectively. The solid lines represent the energy density of the battery, while the dashed lines represent the average ergotropy. Numerical analysis reveals that when the multi-particle quantum battery is coupled to a fermionic thermal reservoir, interparticle interactions J do not enhance its performance, regardless of whether the battery operates in a weak or strong dissipation regime. However, compared to low-temperature conditions, a high-temperature environment significantly improves both the energy storage capacity and the extractable energy of the battery.

Based on the above discussion, regardless of whether the multi-particle quantum battery is placed in a bosonic or fermionic thermal reservoir, both the energy density and the average ergotropy of the multi-particle quantum battery decrease as the interparticle interaction strength J increases. The underlying physical mechanism behind this behavior lies in the interaction-induced splitting of the battery's energy eigenstates. This spectral reconstruction shifts the system away from the resonance, thereby suppressing energy transfer from the charger to the quantum battery. Consequently, interparticle interactions within the battery emerge as a significant obstacle in designing and implementing efficient multiparticle quantum batteries. Additionally, a high-temperature fermionic thermal reservoir provides a stable foundation for building multi-particle quantum batteries.

V. SUMMARY

In this study, we investigate charging models for singleparticle and multi-particle quantum batteries based on homodyne quantum feedback control. In the single-particle model, both the charger and the battery are modeled as two-level atomic systems. Quantum feedback control is applied to the charger during the charging process, enabling energy transfer through the coupling between the charger and the battery. Subsequently, we examined the effects of bosonic and fermionic thermal reservoirs on the performance of the singleparticle quantum battery. The findings reveal the existence of optimal charging parameters for the system. Compared to bosonic thermal reservoirs, fermionic reservoirs at finite temperature facilitate energy storage and extraction more efficiently. Moreover, the battery charging efficiency R improves with increasing temperature. In the multi-particle quantum battery model, the charger is still modeled as a two-level system, while the quantum battery consists of an ensemble of two-level systems. We further analyze the charging process when the multi-particle quantum battery is collectively placed in either a bosonic or fermionic thermal reservoir. Additionally, we investigate the effects of the reservoir temperature T, the interparticle coupling strength J, and the number of particles N on the performance of the multi-particle quantum battery. The results indicate that when the multi-particle quantum battery is placed in a bosonic thermal reservoir, increasing the temperature reduces both the energy density and the average ergotropy, consistent with the behavior observed in the singleparticle quantum battery. Furthermore, expanding the size of the quantum battery in a bosonic thermal reservoir requires satisfying three conditions: a lower thermal reservoir temperature, weak inter-atomic interactions within the battery, and a low dissipation rate of the quantum battery. For the multiparticle quantum battery in a fermionic thermal reservoir, high temperatures still exhibit corresponding advantages in terms of the battery's energy density and average ergotropy. Simultaneously, the conditions for constructing a multi-particle quantum battery are significantly relaxed. Even under strong interparticle interactions and higher battery dissipation rates, the multi-particle quantum battery still maintains relatively high-performance levels in both energy storage and energy extraction under high-temperature conditions.

ACKNOWLEDGEMENTS

This work is supported by the National Natural Science Foundation of China (NSFC) under Grant No. 12174048; Shenyang Ligong University 2024 introduced high-level talent research support funds under Grant No. 1010147001309.

The data that support the findings of this article are openly available [133].

Appendix A: Steady-state solution of the system when the quantum battery is in a bosonic and fermionic thermal reservoir

be written as $\rho(t) = \sum_{i,j=1}^4 \rho_{ij}(t) |i\rangle\langle j|,$ in matrix form,

$$\rho(t) = \begin{pmatrix} \rho_{11}(t) & \rho_{12}(t) & \rho_{13}(t) & \rho_{14}(t) \\ \rho_{21}(t) & \rho_{22}(t) & \rho_{23}(t) & \rho_{24}(t) \\ \rho_{31}(t) & \rho_{32}(t) & \rho_{33}(t) & \rho_{34}(t) \\ \rho_{41}(t) & \rho_{42}(t) & \rho_{43}(t) & \rho_{44}(t) \end{pmatrix}, \tag{A1}$$

To solve Eq. (7), we expand all the operators appearing in it using a global basis set for the two qubits. We choose $|1\rangle = |ee\rangle$, $|2\rangle = |eg\rangle$, $|3\rangle = |ge\rangle$, and $|4\rangle = |gg\rangle$. Accordingly, the density operator $\rho(t)$ of the system at an arbitrary time t can

where ρ_{ij} are the corresponding expansion coefficients. When the quantum battery is in contact with a bosonic thermal reservoir, the differential equations are obtained by solving the corresponding master equation

$$\dot{\rho}_{11}(t) = 2f\rho_{11}(t) - (\Gamma_C + \Gamma_B + n_b\Gamma_B)\rho_{11}(t) + n_b\Gamma_B\rho_{22}(t) + \frac{f^2}{\Gamma_C\eta}[\rho_{33}(t) - \rho_{11}(t)], \tag{A2}$$

$$\dot{\rho}_{22}(t) = 2f\rho_{22}(t) - ig[\rho_{32}(t) - \rho_{23}(t)] - (\Gamma_C + n_b\Gamma_B)\rho_{22}(t) + (1 + n_b)\Gamma_B\rho_{11}(t) + \frac{f^2}{\Gamma_C\eta}[\rho_{44}(t) - \rho_{22}(t)], \tag{A3}$$

$$\dot{\rho}_{33}(t) = -2f\rho_{11}(t) - ig[\rho_{23}(t) - \rho_{32}(t)] + \Gamma_C \rho_{11}(t) - (1 + n_b)\Gamma_B \rho_{33}(t) + n_b\Gamma_B \rho_{44}(t) + \frac{f^2}{\Gamma_C \eta}[\rho_{11}(t) - \rho_{33}(t)], \quad (A4)$$

$$\dot{\rho}_{44}(t) = -2f\rho_{22}(t) + \Gamma_C \rho_{22}(t) + (1+n_b)\Gamma_B \rho_{33}(t) - n_b\Gamma_B \rho_{44}(t) + \frac{f^2}{\Gamma_C \eta} [\rho_{22}(t) - \rho_{44}(t)], \tag{A5}$$

$$\dot{\rho}_{12}(t) = \dot{\rho}_{21}^{*}(t) = 2f\rho_{12}(t) + ig\rho_{13}(t) - \left[\Gamma_C + \left(n_b + \frac{1}{2}\right)\Gamma_B\right]\rho_{12}(t) + \frac{f^2}{\Gamma_C\eta}\left[\rho_{34}(t) - \rho_{12}(t)\right],\tag{A6}$$

$$\dot{\rho}_{13}(t) = \dot{\rho}_{31}^{*}(t) = ig\rho_{12}(t) - \left[\frac{\Gamma_C}{2} + (1+n_b)\Gamma_B\right]\rho_{13}(t) + n_b\Gamma_B\rho_{24}(t) + \left(f - \frac{f^2}{\Gamma_C\eta}\right)[\rho_{31}(t) + \rho_{13}(t)], \quad (A7)$$

$$\dot{\rho}_{14}(t) = \dot{\rho}_{41}^{*}(t) = -\left(\frac{\Gamma_C + \Gamma_B}{2} + n_b \Gamma_B\right) \rho_{14}(t) + \left(f - \frac{f^2}{\Gamma_C \eta}\right) [\rho_{32}(t) + \rho_{14}(t)],\tag{A8}$$

$$\dot{\rho}_{23}(t) = \dot{\rho}_{32}^*(t) = -ig[\rho_{33}(t) - \rho_{22}(t)] - \left(\frac{\Gamma_C + \Gamma_B}{2} + n_b\Gamma_B\right)\rho_{23}(t) + \left(f - \frac{f^2}{\Gamma_C\eta}\right)[\rho_{23}(t) + \rho_{41}(t)], \tag{A9}$$

$$\dot{\rho}_{24}(t) = \dot{\rho}_{42}^*(t) = -ig\rho_{34}(t) - \left(\frac{\Gamma_C}{2} + n_b\Gamma_B\right)\rho_{24}(t) + (1+n_b)\Gamma_B\rho_{13}(t) + \left(f - \frac{f^2}{\Gamma_C\eta}\right)[\rho_{24}(t) + \rho_{42}(t)], \tag{A10}$$

$$\dot{\rho}_{34}(t) = \dot{\rho}_{43}^{*}(t) = (\Gamma_C - 2f)\rho_{12}(t) - ig\rho_{24}(t) - \left[\Gamma_B \left(\frac{1}{2} + n_b\right)\right]\rho_{34}(t) + \frac{f^2}{\Gamma_C \eta}[\rho_{12}(t) - \rho_{34}(t)]. \tag{A11}$$

Then setting $\dot{\rho}(t) = 0$, we obtained the following steady-state solutions

$$\rho_{11}^{\infty} = \frac{4g^2 Q_b^2 + n_b \delta^2 W_b}{(1 + 2n_b) W_b S + 4g^2 [2Q_b + (\Gamma_C + \Gamma_B - 2\Gamma_C \delta)\eta]^2}, \quad \rho_{22}^{\infty} = \frac{4g^2 Q_b \Gamma_C (S - \delta^2) + (1 + n_b)(\delta^2 W_b + 4g^2 Q_b \Gamma_B \eta)}{(1 + 2n_b) W_b S + 4g^2 [2Q_b + (\Gamma_C + \Gamma_B - 2\Gamma_C \delta)\eta]^2}, \quad (A12)$$

$$\rho_{33}^{\infty} = \frac{4g^2 Q_b [(1+n_b)\Gamma_B \eta + \Gamma_C (S-\delta^2)] + n_b W_b (S-\delta^2)}{(1+2n_b)W_b S + 4g^2 [2Q_b + (\Gamma_C + \Gamma_B - 2\Gamma_C \delta)\eta]^2},\tag{A13}$$

$$\rho_{44}^{\infty} = \frac{4g^2\Gamma_C(S - \delta^2) + (1 + n_b)[W_b(S - \delta^2) + 4g^2\Gamma_B\eta]}{(1 + 2n_b)W_bS + 4g^2[2Q_b + (\Gamma_C + \Gamma_B - 2\Gamma_C\delta)\eta]^2},$$
(A14)

$$\rho_{14}^{\infty} = \rho_{41}^{\infty*} = \frac{4ig\delta(\delta - \eta)\Gamma_C^2 \Gamma_B[\delta^2 + n_b(2\delta - 1)\eta]}{(1 + 2n_b)W_bS + 4g^2[2Q_b + (\Gamma_C + \Gamma_B - 2\Gamma_C\delta)\eta]^2},$$
(A15)

$$\rho_{23}^{\infty} = \rho_{32}^{\infty*} = \frac{2ig\Gamma_C \Gamma_B [\delta^2 + n_b(2\delta - 1)\eta] \left\{ 2Q_b + [\Gamma_C (1 - 2\delta) + \Gamma_B]\eta \right\}}{(1 + 2n_b)W_b S + 4g^2 [2Q_b + (\Gamma_C + \Gamma_B - 2\Gamma_C\delta)\eta]^2}.$$
(A16)

We set $\delta=f/\Gamma_C$, $S=2\delta^2+\eta-2\delta\eta$, $Q_b=\Gamma_C\delta^2+n_b\Gamma_B\eta$ and $W_b=\Gamma_C\Gamma_B(\Gamma_C+\Gamma_B+2n_b\Gamma_B)[4Q_b+(\Gamma_C+\Gamma_B-4\Gamma_C\delta-2n_b\Gamma_B)\eta]$ for simplicity. The other steady-state expansion coefficients are all zero, that is $\rho_{12}^{\infty}=\rho_{21}^{\infty}=\rho_{13}^{\infty}=\rho_{31}^{\infty}=\rho_{24}^{\infty}=\rho_{42}^{\infty}=\rho_{34}^{\infty}=\rho_{43}^{\infty}=0$. Combining Eqs. (8) and (10), we obtain the explicit expression for the stored energy and the ergotropy of the quantum battery as follows

$$\mathcal{E}(t) = \frac{\omega_0}{2} \{ \sqrt{4|\rho_{12}(t) + \rho_{34}(t)|^2 + [2(\rho_{11}(t) + \rho_{33}(t)) - 1]^2} + [2(\rho_{11}(t) + \rho_{33}(t)) - 1] \}.$$
(A18)

According to Eqs. (A17) and (A18), the energy storage and the ergotropy of the quantum battery in the steady state can be determined. The expression for the ergotropy of the battery is more complex and will not be provided here, while the expression for energy storage is as follows

$$E_B(\infty) = \omega_0 \frac{n_b W_b S + 4g^2 Q_b [2Q_b + \Gamma_C (1 - 2\delta)\eta + \Gamma_B \eta]}{(1 + 2n_b) W_b S + 4g^2 [2Q_b + \Gamma_C (1 - 2\delta)\eta + \Gamma_B \eta]^2}.$$
(A19)

When the quantum battery is in contact with a fermionic thermal reservoir, the differential equations are similarly obtained by solving the corresponding master equation. By setting $\dot{\rho}(t)=0$, the steady-state solution is obtained as follows

$$E_B(t) = \omega_0[\rho_{11}(t) + \rho_{33}(t)],$$
 (A17)

$$\rho_{11}^{\infty} = \frac{4g^2 Q_f^2 + n_f \delta^2 W_f}{4g^2 (\Gamma_B \eta + \Gamma_C S)^2 + W_f S}, \qquad \rho_{22}^{\infty} = \frac{(1 - n_f) \delta^2 W_f + 4g^2 Q_f [(1 - n_f) \Gamma_B \eta + \Gamma_C (S - \delta^2)]}{4g^2 (\Gamma_B \eta + \Gamma_C S)^2 + W_f S}, \tag{A20}$$

$$\rho_{33}^{\infty} = \frac{n_f(S - \delta^2)W_f + 4g^2Q_f[(1 - n_f)\Gamma_B\eta + \Gamma_C(S - \delta^2)]}{4g^2(\Gamma_B\eta + \Gamma_CS)^2 + W_fS},$$
(A21)

$$\rho_{44}^{\infty} = \frac{(1 - n_f)(S - \delta^2)W_f + 4g^2[(n_f - 1)\Gamma_B\eta - \Gamma_C(S - \delta^2)]^2}{4g^2(\Gamma_B\eta + \Gamma_CS)^2 + W_fS},$$
(A22)

$$\rho_{14}^{\infty} = \rho_{41}^{\infty*} = -\frac{4ig\Gamma_C^2 \delta \Gamma_B (\delta - \eta)[(2n_f - 1)\delta^2 + n_f \eta - 2n_f \delta \eta]}{4g^2 (\Gamma_B \eta + \Gamma_C S)^2 + W_f S},$$
(A23)

$$\rho_{23}^{\infty} = \rho_{32}^{\infty*} = -\frac{2ig\Gamma_C \Gamma_B [(2n_f - 1)\delta^2 + n_f \eta (1 - 2\delta)](\Gamma_B \eta + \Gamma_C S)}{4g^2 (\Gamma_B \eta + \Gamma_C S)^2 + W_f S}.$$
(A24)

We set $\delta=f/\Gamma_C$ for simplicity. The other steady-state expansion coefficients are all zero, i.e. $\rho_{12}^\infty=\rho_{21}^\infty=\rho_{13}^\infty=$

$$\rho_{31}^{\infty}=\rho_{24}^{\infty}=\rho_{42}^{\infty}=\rho_{34}^{\infty}=\rho_{43}^{\infty}=0.$$
 According to Eqs. (A17)

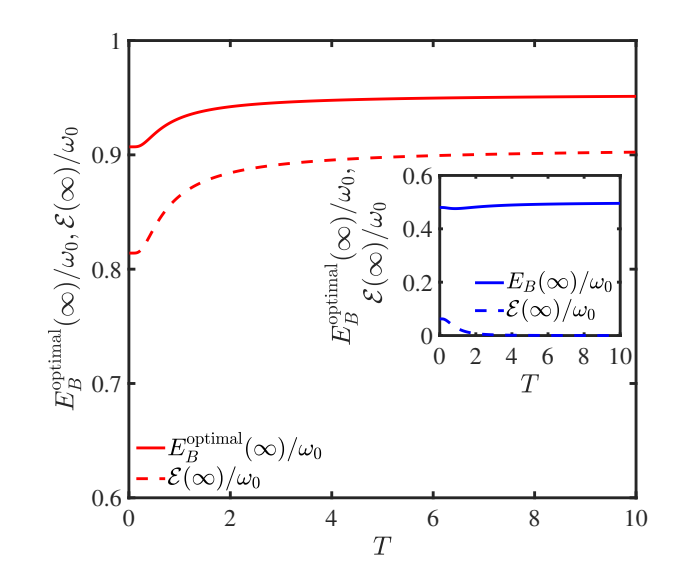


FIG. 22. The steady-state stored energy (solid line) and the ergotropy (dashed line) of the quantum battery are plotted as functions of the fermionic thermal reservoir temperature under optimal charging parameters of $\Gamma_C=2g$ and $\delta=f/\Gamma_C=1$. The coupling strength between the charger and the battery is set to $g=0.01\omega_0$. The red curve represents the results from our proposed scheme. The corresponding results from Ref. [97] are shown as the blue curve in the inset, with the parameter choices matching those in Fig. 5(a) of Ref. [97], i.e., $F=\Gamma_C=4g$.

and (A18), the stored energy and the ergotropy of the quantum battery in steady state can be determined. The expression for the ergotropy of the battery is more complex and will not be provided here, while the expression for energy storage is as follows

$$E_B(\infty) = \omega_0 \frac{4g^2 Q_f (\Gamma_B \eta + \Gamma_C S) + n_f W_f S}{4g^2 (\Gamma_B \eta + \Gamma_C S)^2 + W_f S}, \quad (A25)$$

where
$$\delta=f/\Gamma_C$$
, $S=2\delta^2+\eta-2\delta\eta$, $Q_f=\Gamma_C\delta^2+n_f\Gamma_B\eta$ and $W_f=\Gamma_C\Gamma_B(\Gamma_C+\Gamma_B)[\Gamma_B\eta+\Gamma_C(2S-\eta)]$.

Appendix B: A comparative analysis between the current work and reference [97]

In reference [97], the charger is modeled as a dissipative system embedded in either a bosonic or fermionic thermal reservoir, and powered by a driving laser field, while the quantum battery is isolated. For the case where the charger is embedded in a fermionic thermal reservoir with positive temperatures, we evaluate the quantum battery's performance and conduct a comparative analysis with our proposed scheme. When the system reaches a steady state, the stored energy $E_B(\infty)$ of the battery and the ergotropy $\mathcal{E}(\infty)$ of the battery are

$$E_B(\infty) = \omega_0 \frac{4F^4 g^2 + 2A\Gamma_C^2 + B\Gamma_C^4}{8F^4 g^2 + 4[A + 2g^4(1 - 2n_f)]\Gamma_C^2 + 2[B + 2g^2(1 - 2n_f)]\Gamma_C^4},$$
(B1)

$$\mathcal{E}(\infty) = \frac{\omega_0}{2} \left(-1 + 2\sqrt{\frac{g^2[B + g^2(1 - 4n_f)](1 - 2n_f)^2\Gamma_C^4(2g^2 + \Gamma_C^2)^2}{\{4F^4g^2 + 2[A + 2g^4(1 - 2n_f)]\Gamma_C^2 + [B + 2g^2(1 - 2n_f)]\Gamma_C^4\}^2}} + \frac{4F^4g^2 + 2A\Gamma_C^2 + B\Gamma_C^4}{8F^4g^2 + 4[A + 2g^4(1 - 2n_f)]\Gamma_C^2 + 2[B + 2g^2(1 - 2n_f)]\Gamma_C^4} \right), \tag{B2}$$

where $A=F^2g^2[1-8(n_f-1)n_f]+F^4(1-2n_f)^2+4g^4n_f$, and $B=F^2(1-2n_f)^2+4g^2n_f$. Here, F is the amplitude of the driving field, Γ_C is the dissipation rate of the charger, q is the coupling strength between the charger and the battery, and n_f is the average excitation number of the fermionic thermal reservoir. To better compare the differences between our scheme and that in the Ref. [97], Fig. 22 plots the steady-state stored energy of the quantum battery (red solid line) and its ergotropy (red dashed line) under our charging scheme in a fermionic thermal reservoir as a function of temperature. The corresponding results from Ref. [97] are displayed in the inset, with the parameter choices matching those in Fig. 5(a) of Ref. [97], i.e., F=4g and $\Gamma_C=4g$. Here, the solid line represents the steady-state energy storage of the battery, and the dashed line corresponds to the maximum extractable energy (the ergotropy) of the battery. The results indicate that, in our scheme, both the energy storage and the maximum ex-

tractable energy of the battery increase with the temperature rise. In contrast, the results in Ref. [97] show that, as the temperature increases, the maximum stored energy $E_B^{\rm optimal}(\infty)$ of the quantum battery tends to approach $0.5\omega_0$, and the maximum extractable energy $\mathcal{E}(\infty)$ gradually decreases to zero.

Appendix C: A strongly dissipative multi-particle quantum battery in a bosonic thermal reservoir

In this section, we investigate the dependence of the energy density, the average ergotropy, and the charging efficiency R of the multi-particle quantum battery on three key parameters: the thermal reservoir temperature, the number of particles N and the interatomic interaction strength J, under strong dissipation conditions ($\Gamma_B=0.5g$) in a bosonic thermal reservoir. Figure 23 shows how the energy density

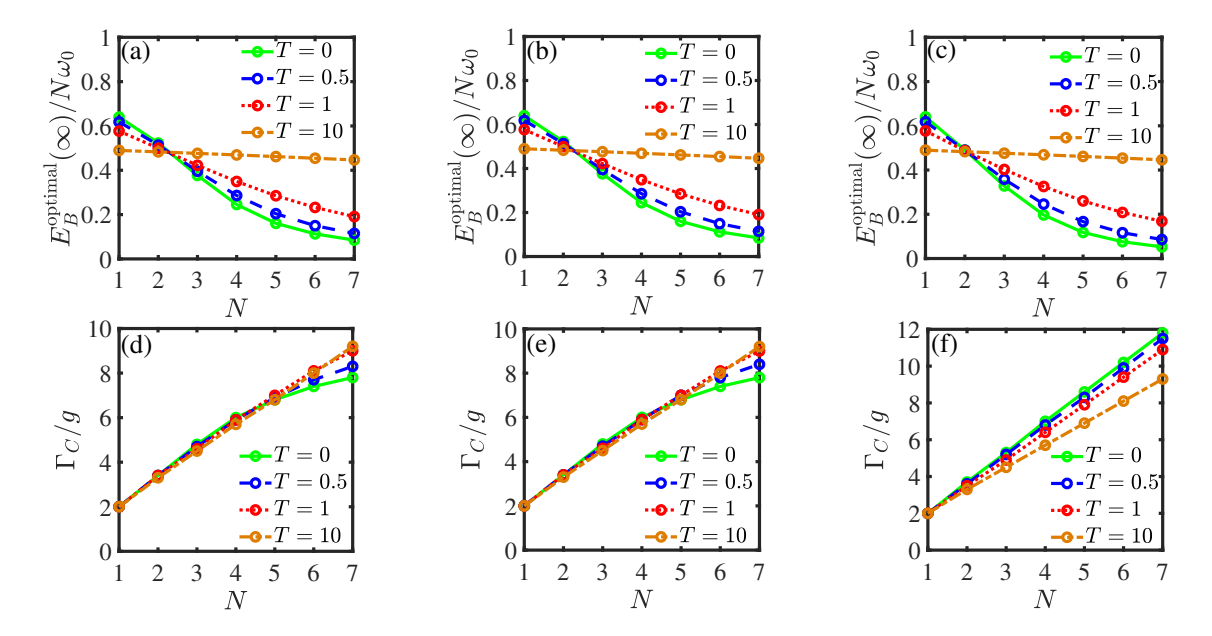


FIG. 23. The multi-particle quantum battery is placed in a bosonic thermal reservoir, with the strong dissipation rate of $\Gamma_B = 0.5g$. The optimal energy density of the battery is plotted as a function of the number of quantum battery particles, under different reservoir temperatures and internal interactions between particles within the battery. The remaining information is provided in Fig. 14.

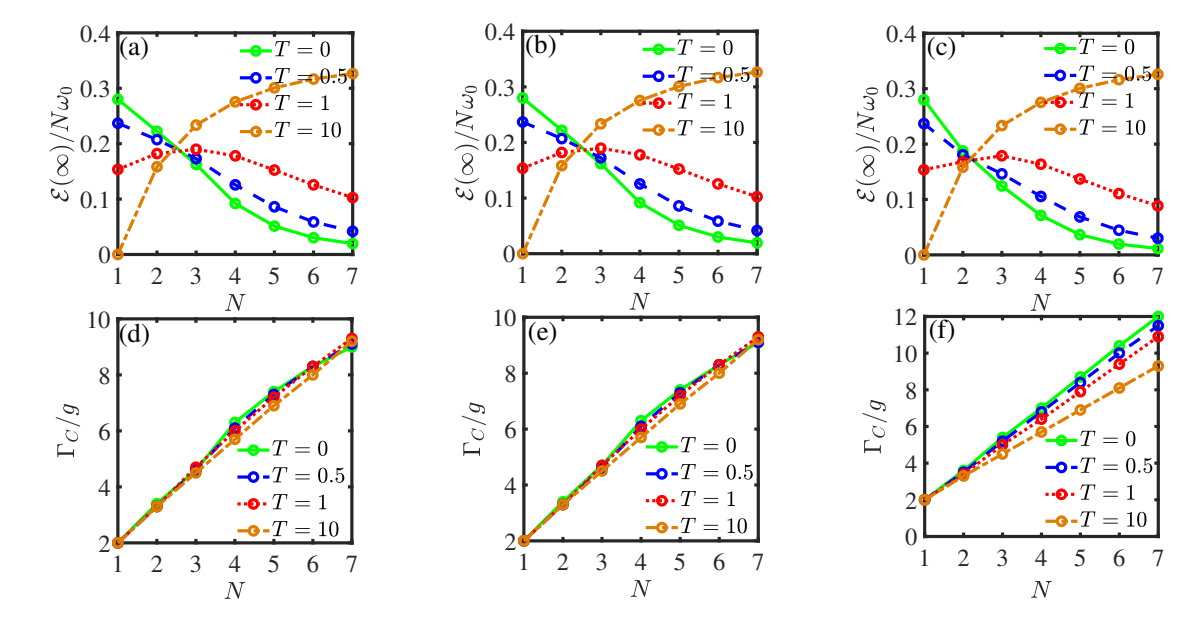
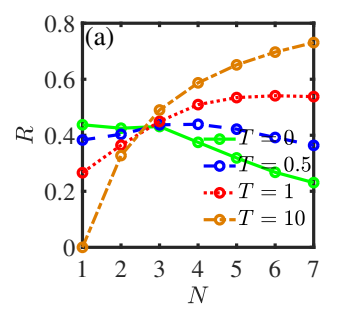
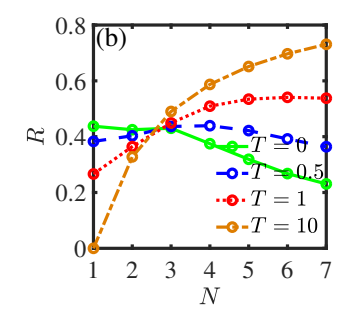


FIG. 24. In a bosonic thermal reservoir, the average ergotropy of the quantum battery in the steady state is shown as a function of the particle number N, where $\Gamma_B = 0.5g$. The remaining information is the same as in Fig. 15.

of the multi-particle quantum battery varies with the particle number N under different temperatures and interatomic interactions within the battery. Panels (a)-(c) correspond to $J=0,\,J=0.1g$, and J=g, respectively, and the different curves represent different thermal reservoir temperatures. Figures 23 (d)-(f) correspond to the optimal dissipative rates of the charger required for Figs. 23 (a)-(c). Unlike the weak dissipation regime depicted in Fig. 14, the strong dissipation regime exhibits a universal decrease in energy density with increasing particle number N, independent of both the ther-

mal reservoir temperature (ranging from low to high) and the strength of interparticle coupling within the battery (whether weak or strong). Consequently, constructing multi-particle quantum batteries in a strongly dissipative bosonic thermal reservoir is not advisable. However, it should be noted that for the number of particles N>2, a high-temperature environment can alleviate the reduction in energy density induced by increasing N. Figure 24 shows correspondingly the behavior of the average ergotropy of the multi-particle quantum battery. The result shows that in a high-temperature environ-





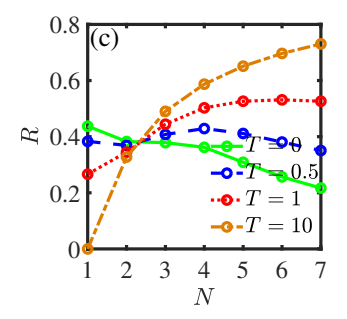


FIG. 25. The multi-particle quantum battery is in a bosonic thermal reservoir. The charging efficiency R of the battery is shown as a function of the number of battery particles N. The remaining information is the same as in Fig. 16.

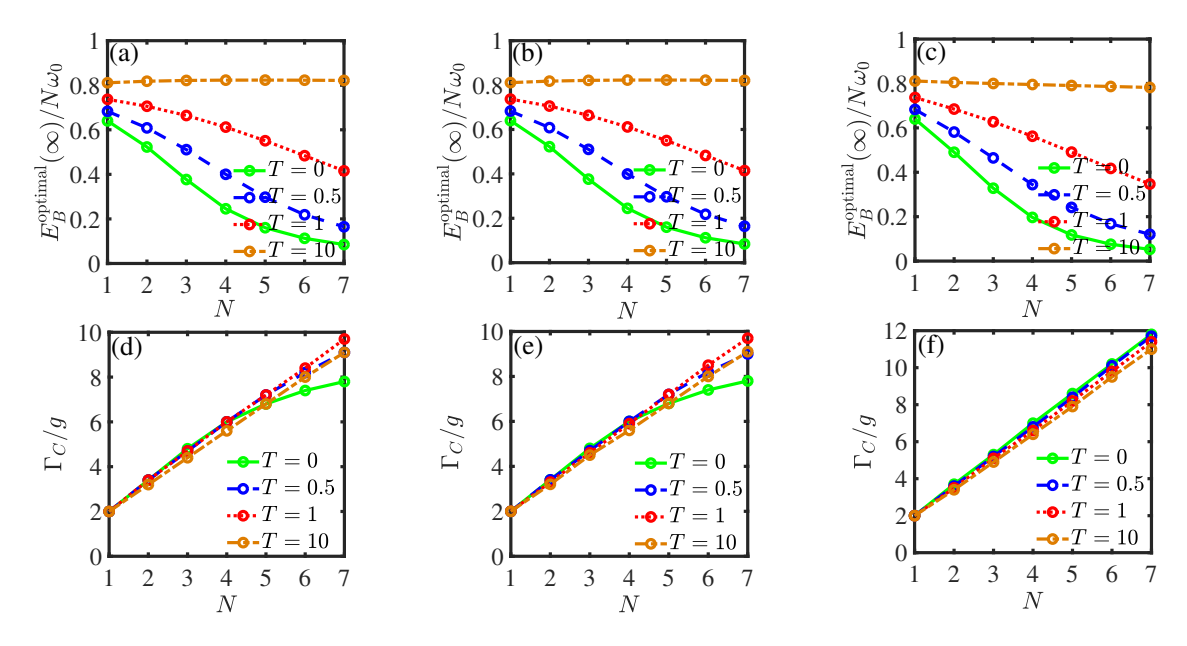


FIG. 26. The multi-particle quantum battery is placed in a fermionic thermal reservoir. The optimal energy density of multi-particle quantum batteries is shown as a function of the particle number N. The only difference from Fig. 18 is that the dissipation rate of the battery is set to $\Gamma_B = 0.5g$.

ment, an increase in the number of particles N is beneficial for energy extraction. Meanwhile, as shown in Fig. 25, the charging efficiency R of the battery increases with the number of particles under high-temperature conditions. In contrast, under low-temperature conditions, R decreases as the number of particles N increases.

Appendix D: A strongly dissipative multi-particle quantum battery in a fermionic thermal reservoir.

When the multi-particle quantum battery operates in a strongly dissipative fermionic thermal reservoir ($\Gamma_B=0.5g$), the energy density of the battery as a function of the number of particles N is shown in Fig. 26. Figures 26 (a)-(c) correspond to J=0, J=0.1g, and J=g, respectively, with different curves representing various temperatures of the thermal reservoir. Figures 26 (d)-(f) show the corresponding optimal dissipative rates of the charger required for the

cases in Fig. 26 (a)-(c), respectively. The results indicate that in a strong fermionic thermal reservoir, an increase in temperature enhances the energy density of the quantum battery. This means that higher temperatures facilitate energy storage in multi-particle quantum batteries. However, increasing the number of particles in the battery under low temperature conditions will have a negative impact on the energy density, regardless of whether the interatomic interaction strength is strong or weak. Conversely, under high-temperature conditions, as the number of battery particles increases, the battery will maintain a state with higher energy density, and the interatomic interaction strength J has a relatively minor influence on its energy density. As shown in Fig. 27, the behavior of the average ergotropy closely resembles that of energy storage. Furthermore, Fig. 28 shows that the charging efficiency R of the battery increases with the number of particles under high-temperature conditions, whereas under low-temperature conditions, R decreases as N increases.

Overall, regardless of whether the multi-particle quantum

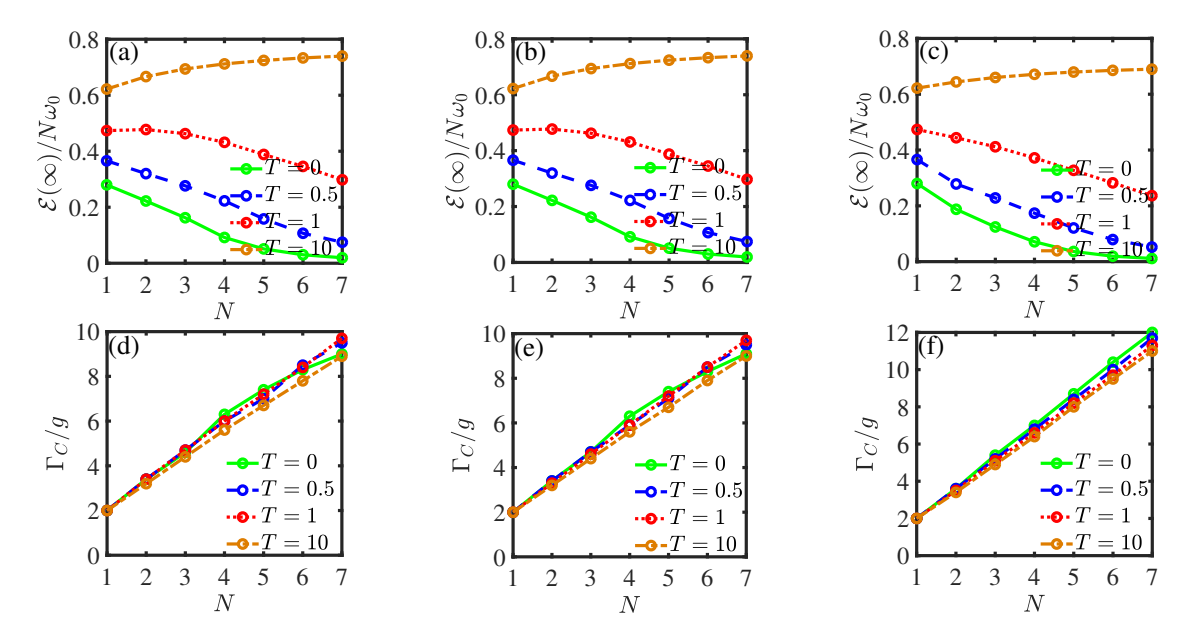


FIG. 27. In a fermionic thermal reservoir, the average ergotropy of the multi-particle quantum battery in the steady state is shown as a function of the particle number N. Except for $\Gamma_B = 0.5g$, all other parameters are the same as in Fig. 19.

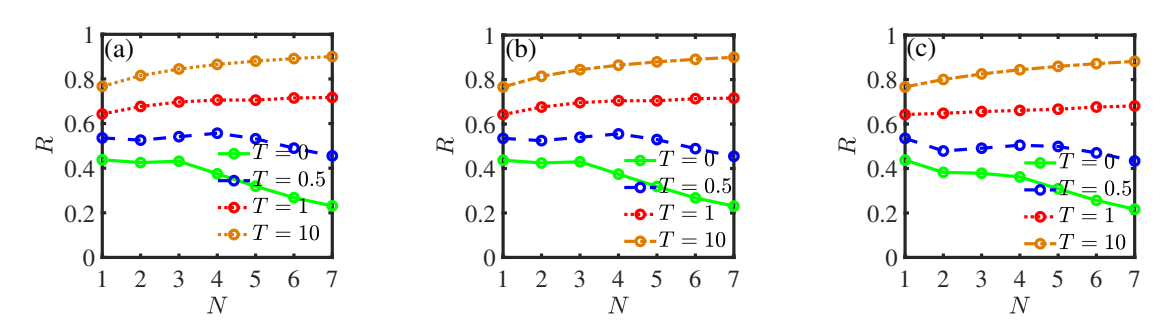


FIG. 28. The multi-particle quantum battery is coupled to a fermionic thermal reservoir. The charging efficiency R of the battery is shown as a function of the number of battery particles N, where $\Gamma_B = 0.5g$, and the other parameters are the same as those in Fig. 20.

battery operates under a low or high dissipation rate, its performance in a high-temperature fermionic thermal reservoir is significantly superior to that of a counterpart constructed in a bosonic thermal reservoir.

R. Alicki and M. Fannes, "Entanglement boost for extractable work from ensembles of quantum batteries," Phys. Rev. E 87, 042123 (2013).

^[2] T. Kanti Konar, L. G. C. Lakkaraju, S. Ghosh, and A. Sen(De), "Quantum battery with ultracold atoms: Bosons versus fermions," Phys. Rev. A 106, 022618 (2022).

^[3] Z. Beleño, M. F. Santos, and F. Barra, "Laser powered dissipative quantum batteries in atom-cavity qed," New. J. Phys 26, 073049 (2024).

^[4] A. Rojo-Francàs, F. Isaule, A. C. Santos, B. Juliá-Díaz, and N. T. Zinner, "Stable collective charging of ultracold-atom quantum batteries," Phys. Rev. A 110, 032205 (2024).

^[5] Y.-Y. Zhang, T.-R. Yang, L. Fu, and X. Wang, "Powerful harmonic charging in a quantum battery," Phys. Rev. E 99, 052106 (2019).

^[6] R. Alicki, "A quantum open system model of molecular bat-

tery charged by excitons," The Journal of Chemical Physics **150**, 5096772 (2019).

^[7] J.-X. Liu, H.-L. Shi, Y.-H. Shi, X.-H. Wang, and W.-L. Yang, "Entanglement and work extraction in the central-spin quantum battery," Phys. Rev. B 104, 245418 (2021).

^[8] L. Peng, W.-B. He, S. Chesi, H.-Q. Lin, and X.-W. Guan, "Lower and upper bounds of quantum battery power in multiple central spin systems," Phys. Rev. A **103**, 052220 (2021).

^[9] P. Chen, T. S. Yin, Z. Q. Jiang, and G. R. Jin, "Quantum enhancement of a single quantum battery by repeated interactions with large spins," Phys. Rev. E 106, 054119 (2022).

^[10] R. Salvia, M. Perarnau-Llobet, G. Haack, N. Brunner, and S. Nimmrichter, "Quantum advantage in charging cavity and spin batteries by repeated interactions," Phys. Rev. Research 5, 013155 (2023).

^[11] H.-Y. Yang, K. Zhang, X.-H. Wang, and H.-L. Shi, "Optimal

- energy storage and collective charging speedup in the centralspin quantum battery," arXiv:2411.01175.
- [12] T. P. Le, J. Levinsen, K. Modi, M. M. Parish, and F. A. Pollock, "Spin-chain model of a many-body quantum battery," Phys. Rev. A 97, 022106 (2018).
- [13] S. Ghosh, T. Chanda, and A. Sen, "Enhancement in the performance of a quantum battery by ordered and disordered interactions," Phys. Rev. A 101, 032115 (2020).
- [14] S. Ghosh, T. Chanda, S. Mal, and A. Sen, "Fast charging of a quantum battery assisted by noise," Phys. Rev. A 104, 032207 (2021).
- [15] S. Ghosh and A. Sen, "Dimensional enhancements in a quantum battery with imperfections," Phys. Rev. A 105, 022628 (2022).
- [16] F.-Q. Dou, H. Zhou, and J.-A. Sun, "Cavity heisenberg-spinchain quantum battery," Phys. Rev. A 106, 032212 (2022).
- [17] R. Grazi, D. Sacco Shaikh, M. Sassetti, N. Traverso Ziani, and D. Ferraro, "Controlling energy storage crossing quantum phase transitions in an integrable spin quantum battery," Phys. Rev. Lett. 133, 197001 (2024).
- [18] F.-Q. Dou and F.-M. Yang, "Superconducting transmon qubitresonator quantum battery," Phys. Rev. A 107, 023725 (2023).
- [19] G. Gemme, M. Grossi, S. Vallecorsa, M. Sassetti, and D. Ferraro, "Qutrit quantum battery: Comparing different charging protocols," Phys. Rev. Research 6, 023091 (2024).
- [20] F.-M. Yang and F.-Q. Dou, "Resonator-qutrit quantum battery," Phys. Rev. A 109, 062432 (2024).
- [21] V. Shaghaghi, V. Singh, G. Benenti, and D. Rosa, "Micromasers as quantum batteries," Quantum Sci. Technol. 7, 04LT01 (2022).
- [22] V. Shaghaghi, V. Singh, M. Carrega, D. Rosa, and G. Benenti, "Lossy micromaser battery: Almost pure states in the jaynes–cummings regime," Entropy **25**, 430 (2023).
- [23] C. Rodríguez, D. Rosa, and J. Olle, "Artificial intelligence discovery of a charging protocol in a micromaser quantum battery," Phys. Rev. A 108, 042618 (2023).
- [24] F. C. Binder, S. Vinjanampathy, K. Modi, and J. Goold, "Quantacell: powerful charging of quantum batteries," New J. Phys. 17, 075015 (2015).
- [25] D. Rossini, G. M. Andolina, D. Rosa, M. Carrega, and M. Polini, "Quantum advantage in the charging process of sachdev-ye-kitaev batteries," Phys. Rev. Lett. 125, 236402 (2020).
- [26] J. Carrasco, J. R. Maze, C. Hermann-Avigliano, and F. Barra, "Collective enhancement in dissipative quantum batteries," Phys. Rev. E 105, 064119 (2022).
- [27] J. Y. Gyhm and U. R. Fischer, "Beneficial and detrimental entanglement for quantum battery charging," Quantum Sci. 6, 0184903 (2024).
- [28] F. Campaioli, F. A. Pollock, F. C. Binder, L. Céleri, J. Goold, S. Vinjanampathy, and K. Modi, "Enhancing the charging power of quantum batteries," Phys. Rev. Lett. 118, 150601 (2017).
- [29] D. Ferraro, M. Campisi, G. M. Andolina, V. Pellegrini, and M. Polini, "High-power collective charging of a solid-state quantum battery," Phys. Rev. Lett. 120, 117702 (2018).
- [30] S. Seah, M. Perarnau-Llobet, G. Haack, N. Brunner, and S. Nimmrichter, "Quantum speed-up in collisional battery charging," Phys. Rev. Lett. 127, 100601 (2021).
- [31] A. Crescente, M. Carrega, M. Sassetti, and D. Ferraro, "Ultrafast charging in a two-photon dicke quantum battery," Phys. Rev. B 102, 245407 (2020).
- [32] J. Y. Gyhm, D. Šafránek, and D. Rosa, "Quantum charging advantage cannot be extensive without global operations," Phys.

- Rev. Lett. 128, 140501 (2022).
- [33] F.-Q. Dou, Y.-Q. Lu, Y.-J. Wang, and J.-A. Sun, "Extended dicke quantum battery with interatomic interactions and driving field," Phys. Rev. B 105, 115405 (2022).
- [34] S. Zakavati, F. T. Tabesh, and S. Salimi, "Bounds on charging power of open quantum batteries," Phys. Rev. E 104, 054117 (2021).
- [35] F. Mayo and A. J. Roncaglia, "Collective effects and quantum coherence in dissipative charging of quantum batteries," Phys. Rev. A 105, 062203 (2022).
- [36] L. Gao, C. Cheng, W.-B. He, R. Mondaini, X.-W. Guan, and H.-Q. Lin, "Scaling of energy and power in a large quantum battery-charger model," Phys. Rev. Research 4, 043150 (2022).
- [37] T. K. Konar, L. G. C. Lakkaraju, and A. Sen, "Quantum battery with non-hermitian charging," Phys. Rev. A 109, 042207 (2024)
- [38] S. Pokhrel and J. Gea-Banacloche, "Large collective power enhancement in dissipative charging of a quantum battery," Phys. Rev. Lett. 134, 130401 (2025).
- [39] S. Mondal and S. Bhattacharjee, "Periodically driven many-body quantum battery," Phys. Rev. E **105**, 044125 (2022).
- [40] S. Julià-Farré, T. Salamon, A. Riera, M. N. Bera, and M. Lewenstein, "Bounds on the capacity and power of quantum batteries," Phys. Rev. Research 2, 023113 (2020).
- [41] W. Lu, J. Chen, L.-M. Kuang, and X. Wang, "Optimal state for a tavis-cummings quantum battery via the bethe ansatz method," Phys. Rev. A **104**, 043706 (2021).
- [42] A. Crescente, D. Ferraro, M. Carrega, and M. Sassetti, "Enhancing coherent energy transfer between quantum devices via a mediator," Phys. Rev. Research 4, 033216 (2022).
- [43] R. R. Rodriguez, B. Ahmadi, P. Mazurek, S. Barzanjeh, R. Alicki, and P. Horodecki, "Catalysis in charging quantum batteries," Phys. Rev. A 107, 042419 (2023).
- [44] T. F. F. Santos, Y. V. de Almeida, and M. F. Santos, "Vacuum-enhanced charging of a quantum battery," Phys. Rev. A 107, 032203 (2023).
- [45] W.-X. Guo, F.-M. Yang, and F.-Q. Dou, "Analytically solvable many-body rosen-zener quantum battery," Phys. Rev. A 109, 032201 (2024).
- [46] M. Alimuddin, T. Guha, and P. Parashar, "Structure of passive states and its implication in charging quantum batteries," Phys. Rev. E 102, 022106 (2020).
- [47] Y.-K. Wang, L.-Z. Ge, T. Zhang, S.-M. Fei, and Z.-X. Wang, "Dynamics of quantum battery capacity under markovian channels," arXiv:2408.03797.
- [48] F. Cavaliere, G. Gemme, G. Benenti, D. Ferraro, and M. Sassetti, "Dynamical blockade of a reservoir for optimal performances of a quantum battery," Commun. Phys. 8, 76 (2025).
- [49] A. Delmonte, A. Crescente, M. Carrega, D. Ferraro, and M. Sassetti, "Characterization of a two-photon quantum battery: Initial conditions, stability and work extraction," Entropy 23, 612 (2021).
- [50] O. Abah, G. De Chiara, M. Paternostro, and R. Puebla, "Harnessing nonadiabatic excitations promoted by a quantum critical point: Quantum battery and spin squeezing," Phys. Rev. Research 4, L022017 (2022).
- [51] M. B. Arjmandi, H. Mohammadi, and A. C. Santos, "Enhancing self-discharging process with disordered quantum batteries," Phys. Rev. E 105, 054115 (2022).
- [52] P. R. Lai, J. D. Lin, Y. T. Huang, H. C. Jan, and Y. N. Chen, "Quick charging of a quantum battery with superposed trajectories," Phys. Rev. Research 6, 023136 (2024).
- [53] G. M. Andolina, M. Keck, A. Mari, M. Campisi, V. Giovan-

- netti, and M. Polini, "Extractable work, the role of correlations, and asymptotic freedom in quantum batteries," Phys. Rev. Lett. **122**, 047702 (2019).
- [54] F. Barra, "Dissipative charging of a quantum battery," Phys. Rev. Lett. 122, 210601 (2019).
- [55] F. Barra, K. V. Hovhannisyan, and A. Imparato, "Quantum batteries at the verge of a phase transition," New J. Phys. 24, 015003 (2022).
- [56] B. Aparajita, D. Pratha, and S. Ujjwal, "Nonlinearity-assisted advantage for charger-supported open quantum batteries," arXiv:2410.00618.
- [57] S. Elghaayda, A. Ali, S. Al-Kuwari, A. Czerwinski, M. Mansour, and S. Haddadi, "Performance of a superconducting quantum battery," arXiv:2411.19247.
- [58] F. Pirmoradian and K. Mølmer, "Aging of a quantum battery," Phys. Rev. A 100, 043833 (2019).
- [59] D. Farina, G. M. Andolina, A. Mari, M. Polini, and V. Giovannetti, "Charger-mediated energy transfer for quantum batteries: An open-system approach," Phys. Rev. B 99, 035421 (2019).
- [60] G. Bhanja, D. Tiwari, and S. Banerjee, "Impact of non-markovian quantum brownian motion on quantum batteries," Phys. Rev. A 109, 012224 (2024).
- [61] A. Ali, S. Al-Kuwari, M. T. Hussain, T. Byrnes, M. T. Rahim, J. Q. Quach, M. Ghominejad, and S. Haddadi, "Ergotropy and capacity optimization in heisenberg spin-chain quantum batteries," Phys. Rev. A 110, 052404 (2024).
- [62] J. Q. Quach, K. E. McGhee, L. Ganzer, D. M. Rouse, B. W. Lovett, E. M. Gauger, J. Keeling, G. Cerullo, D. G. Lidzey, and T. Virgili, "Superabsorption in an organic microcavity: Toward a quantum battery," Science advances 8, eabk3160 (2022).
- [63] G. Gemme, M. Grossi, D. Ferraro, S. Vallecorsa, and M. Sassetti, "Ibm quantum platforms: A quantum battery perspective," Batteries 8, 43 (2022).
- [64] J. Joshi and T. S. Mahesh, "Experimental investigation of a quantum battery using star-topology nmr spin systems," Phys. Rev. A 106, 042601 (2022).
- [65] C.-K. Hu, J. Qiu, P. J. P. Souza, J. Yuan, Y. Zhou, L. Zhang, J. Chu, X. Pan, L. Hu, J. Li, Y. Xu, Y. Zhong, S. Liu, F. Yan, D. Tan, R. Bachelard, C. J. Villas-Boas, A. C. Santos, and D.Yu, "Optimal charging of a superconducting quantum battery," Quantum Sci. Technol. 7, 045018 (2022).
- [66] I. M. de Buy Wenniger, S. E. Thomas, M. Maffei, S. C. Wein, M. Pont, A. Harouri, A. Lemaître, I. Sagnes, N. Somaschi, A. Auffèves, and P. Senellart-Mardon, "Coherence-powered work exchanges between a solid-state qubit and light fields," Phys. Rev. Lett. 131, 260401 (2023).
- [67] D. Qu, X. Zhan, H. Lin, and P. Xue, "Experimental optimization of charging quantum batteries through a catalyst system," Phys. Rev. B 108, L180301 (2023).
- [68] F. Campaioli, S. Gherardini, J. Q. Quach, M. Polini, and G. M. Andolina, "Colloquium: quantum batteries," Rev. Mod. Phys. 96, 031001 (2024).
- [69] L. Razzoli, G. Gemme, I. Khomchenko, M. Sassetti, H. Ouer-dane, D. Ferraro, and G. Benenti, "Cyclic solid-state quantum battery: thermodynamic characterization and quantum hardware simulation," Quantum Sci. Technol. 10, 015064 (2025).
- [70] Zhi-Guang Lu, Guoqing Tian, Xin-You Lü, and Cheng Shang, "Topological quantum batteries," Phys. Rev. Lett. 134, 180401 (2025).
- [71] A. C. Santos, B. Çakmak, S. Campbell, and N. T. Zinner, "Stable adiabatic quantum batteries," Phys. Rev. E 100, 032107 (2019).

- [72] A. C. Santos, A. Saguia, and M. S. Sarandy, "Stable and charge-switchable quantum batteries," Phys. Rev. E 101, 062114 (2020).
- [73] F. Caravelli, G. Coulter-De Wit, L. P. García-Pintos, P. Luis, and A. Hamma, "Random quantum batteries," Phys. Rev. Research 2, 023095 (2020).
- [74] F.-Q. Dou, Y.-J. Wang, and J.-A. Sun, "Highly efficient charging and discharging of three-level quantum batteries through shortcuts to adiabaticity," Front. Phys. 17, 1–9 (2022).
- [75] M. Gumberidze, M. Kolář, and R. Filip, "Measurement induced synthesis of coherent quantum batteries," Sci Rep 9, 19628 (2019).
- [76] S. Gherardini, F. Campaioli, F. Caruso, and F. C. Binder, "Stabilizing open quantum batteries by sequential measurements," Phys. Rev. Research 2, 013095 (2020).
- [77] D. Morrone, M. A. C. Rossi, and M. G. Genoni, "Daemonic ergotropy in continuously monitored open quantum batteries," Phys. Rev. Applied 20, 044073 (2023).
- [78] T. Zhang, H. Yang, and S.-M. Fei, "Local-projective-measurement-enhanced quantum battery capacity," Phys. Rev. A 109, 042424 (2024).
- [79] P. Chaki, A. Bhattacharyya, K. Sen, and U. Sen, "Positive and non-positive measurements in energy extraction from quantum batteries," arXiv:2404.18745.
- [80] M. T. Mitchison, J. Goold, and J. Prior, "Charging a quantum battery with linear feedback control," Quantum 5, 500 (2021).
- [81] Y. Yao and X. Q. Shao, "Stable charging of a rydberg quantum battery in an open system," Phys. Rev. E 104, 044116 (2021).
- [82] Y. Yao and X. Q. Shao, "Optimal charging of open spinchain quantum batteries via homodyne-based feedback control," Phys. Rev. E 106, 014138 (2022).
- [83] F. Mazzoncini, V. Cavina, G. M. Andolina, P. A. Erdman, and V. Giovannetti, "Optimal control methods for quantum batteries," Phys. Rev. A 107, 032218 (2023).
- [84] R. R. Rodriguez, B. Ahmadi, G. Suárez, P. Mazurek, S. Barzanjeh, and P. Horodecki, "Optimal quantum control of charging quantum batteries," New J. Phys. 26, 043004 (2024).
- [85] S.-Y. Bai and J.-H. An, "Floquet engineering to reactivate a dissipative quantum battery," Phys. Rev. A 102, 060201 (2020).
- [86] F. T. Tabesh, F. H. Kamin, and S. Salimi, "Environment-mediated charging process of quantum batteries," Phys. Rev. A 102, 052223 (2020).
- [87] F. H. Kamin, F. T. Tabesh, S. Salimi, F. Kheirandish, and A. C. Santos, "Non-markovian effects on charging and selfdischarging process of quantum batteries," New J. Phys. 22, 083007 (2020).
- [88] K. Xu, H.-J. Zhu, G.-F. Zhang, and W.-M. Liu, "Enhancing the performance of an open quantum battery via environment engineering," Phys. Rev. E 104, 064143 (2021).
- [89] S. Qi and J. Jing, "Magnon-mediated quantum battery under systematic errors," Phys. Rev. A 104, 032606 (2021).
- [90] F. Zhao, F.-Q. Dou, and Q. Zhao, "Quantum battery of interacting spins with environmental noise," Phys. Rev. A 103, 033715 (2021).
- [91] K. Xu, H.-G. Li, Z.-G. Li, H.-J. Zhu, G.-F. Zhang, and W.-M. Liu, "Charging performance of quantum batteries in a double-layer environment," Phys. Rev. A **106**, 012425 (2022).
- [92] D. Morrone, M. A. C. Rossi, A. Smirne, and M. G. Genoni, "Charging a quantum battery in a non-markovian environment: a collisional model approach," Quantum Sci. Technol. 8, 035007 (2023).
- [93] B. Mojaveri, R. Jafarzadeh Bahrbeig, M. A. Fasihi, and S. Babanzadeh, "Enhancing the direct charging performance of an

- open quantum battery by adjusting its velocity," Sci Rep 13, 19827 (2023).
- [94] W.-L. Song, H.-B. Liu, B. Zhou, W.-L. Yang, and J.-H. An, "Remote charging and degradation suppression for the quantum battery," Phys. Rev. Lett. 132, 090401 (2024).
- [95] B. Ahmadi, P. Mazurek, P. Horodecki, and Shabir S. Barzanjeh, "Nonreciprocal quantum batteries," Phys. Rev. Lett. 132, 210402 (2024).
- [96] B. Ahmadi, P. Mazurek, S. Barzanjeh, and P. Horodecki, "Super-optimal charging of quantum batteries via reservoir engineering," arXiv:2407.16553.
- [97] M.-L. Song, X.-K. Song, L. Ye, and D. Wang, "Evaluating extractable work of quantum batteries via entropic uncertainty relations," Phys. Rev. E 109, 064103 (2024).
- [98] F. H. Kamin, S. Salimi, and M. B. Arjmandi, "Steady-state charging of quantum batteries via dissipative ancillas," Phys. Rev. A 109, 022226 (2024).
- [99] J. Q. Quach and W. J. Munro, "Using dark states to charge and stabilize open quantum batteries," Phys. Rev. Applied 14, 024092 (2020).
- [100] C. Cruz, M. F. Anka, M. S. Reis, R. Bachelard, and A. C. Santos, "Quantum battery based on quantum discord at room temperature," Quantum Sci. Technol. 7, 025020 (2022).
- [101] E. Artacho and L. M. Falicov, "Open fermionic quantum systems," Phys. Rev. B 47, 1190 (1993).
- [102] W.-M. Zhang, P.-Y. Lo, H.-N. Xiong, M. W. Y. Tu, and F. Nori, "General non-markovian dynamics of open quantum systems," Phys. Rev. Lett. 109, 170402 (2012).
- [103] M. Chen and J. Q. You, "Non-markovian quantum state diffusion for an open quantum system in fermionic environments," Phys. Rev. A 87, 052108 (2013).
- [104] A. Nüßeler, I. Dhand, S. F. Huelga, and M. B. Plenio, "Efficient simulation of open quantum systems coupled to a fermionic bath," Phys. Rev. B 101, 155134 (2020).
- [105] L. Del Re, B. Rost, A. F. Kemper, and J. K. Freericks, "Driven-dissipative quantum mechanics on a lattice: Simulating a fermionic reservoir on a quantum computer," Phys. Rev. B 102, 125112 (2020).
- [106] T. Barthel and Y. Zhang, "Solving quasi-free and quadratic lindblad master equations for open fermionic and bosonic systems," J. Stat. Mech. 2022, 113101 (2022).
- [107] P. Li and B. Jia, "Particle-exchange heat engine working between bosonic and fermionic reservoirs," Phys. Rev. E 83, 062104 (2011).
- [108] A. Ghosh, S. S. Sinha, and D. S. Ray, "Fermionic oscillator in a fermionic bath," Phys. Rev. E 86, 011138 (2012).
- [109] S. Brodbeck, H. Suchomel, M. Amthor, T. Steinl, M. Kamp, C. Schneider, and S. Hoefling, "Observation of the transition from lasing driven by a bosonic to a fermionic reservoir in a gaas quantum well microcavity," Phys. Rev. Lett. 117, 127401 (2016).
- [110] D. Malz and A. Nunnenkamp, "Current rectification in a double quantum dot through fermionic reservoir engineering," Phys. Rev. B 97, 165308 (2018).
- [111] G. G. Damas, R. J. de Assis, and N. G. de Almeida, "Cooling with fermionic thermal reservoirs," Phys. Rev. E 107, 034128 (2023).
- [112] L. Magazzù, E. Paladino, and M. Grifoni, "Unified diagrammatic approach to quantum transport in few-level junctions for bosonic and fermionic reservoirs: Application to the quantum rabi model," Phys. Rev. B 110, 085419 (2024).
- [113] H. M. Wiseman and G. J. Milburn, "Quantum theory of op-

- tical feedback via homodyne detection," Phys. Rev. Lett. **70**, 548–551 (1993).
- [114] H. M. Wiseman, "Quantum theory of continuous feedback," Phys. Rev. A 49, 2133–2150 (1994).
- [115] H. Carmichael, *An open systems approach to quantum optics* (Springer Science & Business Media, 2009).
- [116] P. P. Hofer, M. Perarnau-Llobet, L. D. M. Miranda, G. Haack, R. Silva, J. B. Brask, and N. Brunner, "Markovian master equations for quantum thermal machines: local versus global approach," New J. Phys. 19, 123037 (2017).
- [117] P. P. Potts, A. A. S. Kalaee, and A. Wacker, "A thermodynamically consistent markovian master equation beyond the secular approximation," New J. Phys. 23, 123013 (2021).
- [118] G. Blasi, S. Khandelwal, and G. Haack, "Exact finite-time correlation functions for multiterminal setups: Connecting theoretical frameworks for quantum transport and thermodynamics," Phys. Rev. Research 6, 043091 (2024).
- [119] H. M. Wiseman and G. J. Milburn, *Quantum Measurement and Control* (Cambridge University Press, 2009).
- [120] L. D. Carr, "Negative temperatures?" Science 339, 42 (2013).
- [121] S. Braun, J. P. Ronzheimer, M. Schreiber, S. S. Hodgman, T. Rom, I. Bloch, and U. Schneider, "Negative absolute temperature for motional degrees of freedom," Science 339, 52 (2013).
- [122] D. Frenkel and P. B. Warren, "Gibbs, boltzmann, and negative temperatures," Am. J. Phys. 83, 163–170 (2015).
- [123] E. Abraham and O. Penrose, "Physics of negative absolute temperatures," Phys. Rev. E **95**, 012125 (2017).
- [124] H. Struchtrup, "Work storage in states of apparent negative thermodynamic temperature," Phys. Rev. Lett. 120, 250602 (2018).
- [125] Y. Hama, W. J. Munro, and K. Nemoto, "Relaxation to negative temperatures in double domain systems," Phys. Rev. Lett. 120, 060403 (2018).
- [126] R. J. De Assis, C. J. Villas-Boas, and N. G. de Almeida, "Feasible platform to study negative temperatures," J. Phys. B: At. Mol. Opt. Phys. 52, 065501 (2019).
- [127] Y. Hama, E. Yukawa, W. J. Munro, and K. Nemoto, "Negative-temperature-state relaxation and reservoir-assisted quantum entanglement in double-spin-domain systems," Phys. Rev. A 98, 052133 (2018).
- [128] T. M. Mendonça, A. M. Souza, R. J. de Assis, de N. G. Almeida, R. S. Sarthour, I. S. Oliveira, and C. J. Villas-Boas, "Reservoir engineering for maximally efficient quantum engines," Phys. Rev. Research 2, 043419 (2020).
- [129] A. E. Allahverdyan, R. Balian, and Th. M. Nieuwenhuizen, "Maximal work extraction from finite quantum systems," Europhys. Lett. 67, 565 (2004).
- [130] G. Francica, J. Goold, F. Plastina, and M. Paternostro, "Daemonic ergotropy: Enhanced work extraction from quantum correlations," npj Quantum Inf 3, 12 (2017).
- [131] W. Pusz and S. L. Woronowicz, "Passive states and kms states for general quantum systems," Commun. Math. Phys. 58, 273–290 (1978).
- [132] A. Lenard, "Thermodynamical proof of the gibbs formula for elementary quantum systems," J. Stat. Phys. 19, 575–586 (1978).
- [133] Y. Yao and X. Q. Shao, "Figshare data repository," (2025), https://doi.org/10.6084/m9.figshare.28395878.v4.